Transient proliferation by reversible YAP-mediated increase of the cyclin D1/p27 ratio

Katherine R. Ferrick[1,2], Yilin Fan[1,2,3], Nalin Ratnayeke[1,2,4], Mary N. Teruel[5], Tobias Meyer[1,2,6,*]

[1]Department of Cell and Developmental Biology, Weill Cornell Medicine, New York, NY, USA
[2]Department of Chemical and Systems Biology, Stanford Medicine, Stanford, CA, USA
[3]Current: Department of Pathology and Center for Cancer Research, Massachusetts General Hospital and Harvard Medical School, Boston, MA, USA
[4]Current: Cancer Biology and Genetics Program, Sloan Kettering Institute, Memorial Sloan Kettering Cancer Center, New York, NY, USA
[5]Department of Biochemistry, Weill Cornell Medicine, New York, NY, USA
[6]Lead contact
[*]Correspondence: tom4003@med.cornell.edu

HIGHLIGHTS

- YAP signaling controls cell cycle entry and exit by up- and down-regulating the cyclin D1/p27 ratio above and below a conserved threshold
- YAP-induced proliferation is intrinsically transient since contact inhibition of YAP suppresses EGFR signaling after a delay to reduce this cyclin D1/p27 ratio
- YAP can still be robustly inhibited after Merlin/NF2 ablation but only at higher local cell density
- The YAP-regulated cyclin D1/p27 ratio is primarily controlled by MEK-ERK rather than mTOR activity

SUMMARY

Hippo-YAP signaling orchestrates epithelial tissue repair and is therefore an attractive target in regenerative medicine. Yet it is unresolved how YAP controls the underlying transient proliferative response. Here we show that YAP-TEAD activation increases the nuclear cyclin D1/p27 protein ratio in G1 phase, towards a threshold level that dictates whether individual cells enter or exit the cell cycle. YAP increases this ratio indirectly, by increasing EGFR and other receptor activities that signal primarily through ERK. Conversely, contact inhibition suppresses YAP activity which gradually downregulates mitogen signaling and the cyclin D1/p27 ratio. Increasing YAP activity by ablating the suppressor Merlin/NF2 reveals a robust balancing mechanism in which YAP can still be inhibited after cell division further increases local cell density. Thus, critical for tissue repair, the proliferation response is intrinsically transient since the YAP-induced and mitogen-mediated increase in the cyclin D1/p27 ratio is reliably reversed through delayed contact inhibition of YAP.

INTRODUCTION

Acute chemical and physical injury inactivates the Hippo pathway, which activates the transcriptional cofactor YAP to increase proliferation, along with inducing metabolic changes and matrix remodeling[1,2]. YAP activation initiates transcription by binding TEAD and other nuclear transcription factors[3]. While YAP and its paralog TAZ are dispensable for the basal proliferation of several tissues, they are crucial for regeneration and repair following injury in tissues such as skin, liver, and kidney[1]. Inhibitors of Hippo pathway proteins are therefore being developed for potential clinical use in tissue repair[4–6].

Hippo signaling is kept active in epithelial sheets and other tissues by cell-cell contacts, such as adherens and tight junctions, and is inactivated by mechanical stress during tissue repair[1,7,8]. Adaptor proteins like Merlin (NF2) contribute to contact inhibition signaling to activate LATS1/2, which is the principal kinase of the Hippo pathway suppressing YAP-TEAD activity[9,10]. Consequently, loss of LATS activity leads to dramatic increases in the size of tissues and organs, and tumorigenesis[9,11,12]. Despite the general finding that YAP activation promotes proliferation, the mechanism how YAP initiates cell cycle entry is unresolved.

Different mechanisms have been described through which YAP signaling could increase proliferation. Constitutive YAP activation increases expression of a broad array of cell cycle genes, including DNA replication factors and regulators of G2/M progression[13–15]. YAP also promotes secretion of mitogens[16,17] and cooperates with AP-1 transcription factors in inducing

target genes[15,18,19]. Likewise, cell cycle entry is regulated by both receptor signaling and contact inhibition, which may signal independently of YAP[20,21]. Nevertheless, cell cycle entry is ultimately controlled by cyclin-dependent kinase (CDK) activity in G1 phase which must phosphorylate and inactivate retinoblastoma protein (Rb), the suppressor of the cell cycle transcription factor E2F. How YAP controls Rb phosphorylation in G1 is not established: YAP could induce cell cycle entry by directly regulating cyclin D, indirectly through regulating mitogen signaling, or by reprogramming the cell state.

As persistent YAP activation induces organ hyperplasia and cancer, YAP-TEAD must also be robustly inactivated after the tissue repair is completed. Hippo-dependent and Hippo-independent pathways have been described that can inactivate YAP through phosphorylation, cytoplasmic sequestration, and degradation[3]. The complexity of both the proliferation initiation and termination, together with additional roles of YAP in cell differentiation and cell metabolism, has made it challenging to use animal models to determine how Hippo-YAP signaling coordinates a proliferation response that must be transient, generating only the cells needed to recover the original tissue size during repair.

Here we use multiplexed, single-cell immunofluorescence analysis to examine YAP-regulated proliferation in thousands of epithelial cells in a monolayer. We show that over a wide range of stimuli, proliferation is controlled through a balance mechanism whereby mitogen signaling is opposed by contact inhibition suppressing YAP activity. YAP activation drives proliferation by both increasing the nuclear ratio of the protein level of cyclin D1 and decreasing the level of the CDK inhibitor p27. Strikingly, YAP-activated cells only enter the cell cycle if the cyclin D1/p27 ratio exceeds a critical threshold level during the G1 phase, whereas cells arrest the cell cycle below this threshold. YAP activation increases this cyclin D1/p27 ratio indirectly by increasing the activity of EGFR and other surface receptors, which in turn signal primarily through MEK-ERK, rather than the often-implicated mTOR pathway. Ensuring a strong proliferation response, this inactivation of YAP downregulated EGFR signaling to lower the cyclin D1/p27 ratio, but only after a delay. Ensuring robust YAP signal termination, even a strong increase in YAP activity generated by ablation of the upstream Hippo component Merlin could still be reversed by contact inhibition-mediated YAP inactivation, but only at higher local cell density. Together, our study identifies a balancing mechanism centered on an increase and delayed decrease in the cyclin D1/p27 ratio that makes YAP-induced proliferation intrinsically transient, which is essential for generating a commensurate number of new cells during repair.

RESULTS

92

93 **Contact inhibition of YAP opposes mitogen stimulation in a balance mechanism**
94 **controlling cell proliferation**

95 Even within epithelial monolayers subject to the same mitogen stimuli, there is considerable
96 heterogeneity in cell cycle signaling[22–24] . We therefore used single cell analysis to distinguish
97 between various plausible mechanisms of how YAP activation might be linked to contact
98 inhibition and mitogen signaling to control cell cycle entry. While YAP and TAZ both promote
99 proliferation, we focus here primarily on YAP as it is generally the limiting component in
100 regulating proliferation[13,14]. We used hTERT-immortalized human retinal pigmented epithelial
101 cells (RPE1) that reversibly arrest the cell cycle with serum starvation or contact inhibition[22]. We
102 use the terms “contact inhibition” and “local cell density” interchangeably since the local cell
103 density in monolayers closely predicts whether proliferation is suppressed in individual RPE1
104 cells[22]. We used different concentrations of serum (fetal bovine) to understand the role of
105 mitogens in the process.

106 We quantified local cell density by subdividing segmented nuclei for each image into a
107 10 x 10 grid (~75 x 75 μm) and counting the cells within each block (Figure 1A). Each cell was
108 then assigned its local density based on the number of cells in its block (Figure S1A, see also
109 STAR Methods). To assess changes in proliferation, we measured both phosphorylation of
110 retinoblastoma protein (p-Rb, S807/811), which is a bimodal marker of cyclin-CDK activity[25] that
111 is low in arrested cells and remains high in cycling cells from G1 through mitosis, and EdU
112 incorporation into DNA, which occurs during DNA replication in S phase (Figure 1B, S1B).

113 We first confirmed that increasing the mitogen stimulus from low (0.1% serum) and
114 intermediate (1% serum) to high (10% serum) levels increased the percentage of proliferating
115 cells using both metrics of proliferation, p-Rb (Figure 1C) and EdU (Figure S1C). The proportion
116 of proliferating cells progressively decreased as local cell density increased for high and low
117 serum levels, supporting that mitogen signaling and contact inhibition oppose each other in
118 regulating proliferation. This conclusion was also supported by an alternative metric of local cell
119 density that was based on the area of neighboring cell nuclei[22] within a radius of similar scaling
120 (Figure S1D). This inverse regulation represents an intuitive balancing mechanism: the inhibition
121 of proliferation at a given cell density can be overcome by increasing mitogen signaling, and the
122 increase in proliferation after increasing mitogen signaling can be antagonized once cell division
123 has increased local cell density.

124 We next determined how YAP activity changes this balance between mitogen signaling
125 and contact inhibition by stably expressing a doxycycline (DOX)-inducible, constitutively active

126 YAP variant (5 regulatory serines mutated to alanine[26], CA-YAP). As leaky expression of CA-
127 YAP (without DOX induction) was sufficient to increase proliferation (at a similar expression
128 level compared to the endogenous YAP, Figure S1E), we did not use DOX induction unless
129 otherwise stated. Even with this weaker YAP expression, the cell density dependence of
130 proliferation was abolished in CA-YAP cells (Figure 1C), demonstrating that contact inhibition of
131 proliferation requires contact inhibition of YAP activity. Moreover, CA-YAP cells retained
132 mitogen sensitivity independent of contact inhibition since increasing serum levels further
133 increased the percentage of proliferating cells (Figure 1D, S1F).
134 We next tested whether contact inhibition and mitogen signaling regulate endogenous
135 YAP activity. As the ratio of the nuclear to cytoplasmic (n/c) YAP and the absolute nuclear level
136 of YAP are both relative measures of YAP activity[27,28], we measured both parameters as a
137 function of local cell density (Figure 1E, see also STAR Methods). At 0.1% serum, we observed
138 the expected inhibition of YAP at increasing cells density when monitoring the YAP n/c ratio or
139 the nuclear YAP level. At 1% and 10% serum, the YAP n/c ratio was diminished at higher cell
140 densities, but the nuclear level of YAP was higher than for low serum conditions.
141 We used this single-cell data to analyze the percent of cells with phosphorylated Rb as a
142 function of the relative YAP activity. Markedly, using both metrics, increasing serum levels
143 increased proliferation for cells with identical YAP levels (Figure 1F). Thus, YAP activation and
144 mitogen stimuli synergistically increase proliferation, and exogenously added mitogens increase
145 proliferation directly without requiring increased YAP.
146 Finally, we determined how acute increases and decreases in YAP activity regulate Rb
147 phosphorylation. Using recently developed inhibitors, we inhibited YAP-TEAD signaling with a
148 pan-TEAD inhibitor[29], and activated endogenous YAP using a LATS1/2 inhibitor[5,30]. We
149 confirmed that TEAD inhibition promoted a strong cytoplasmic localization of endogenous YAP
150 while LATS inhibition triggered its nuclear enrichment (Figure 1G). TEAD inhibition greatly
151 reduced the fraction of proliferating cells for low but not for high serum stimuli, suggesting that
152 YAP-TEAD activity is particularly critical for inducing proliferation for low mitogen stimulation
153 conditions (Figure 1H, S1G). Conversely, LATS inhibition greatly boosted proliferation at low
154 serum stimuli and had a smaller relative effect at high serum stimuli due to the already high
155 percentage of proliferating cells (Figure S1H). Finally, this analysis showed that high mitogens
156 can induce proliferation independently of YAP-TEAD activity since TEAD inhibition could
157 reverse the portion of proliferation induced by YAP but not a YAP-independent component of
158 mitogen-induced proliferation (Figure 1H).

159 Together, these experiments strongly support a model that contact inhibition of YAP
160 activity and mitogen signaling compete to respectively suppress or promote proliferation over a
161 wide range of cell densities and mitogen stimuli. However, this balance can be broken in two
162 ways: by high mitogen stimuli inducing proliferation in cells lacking YAP-TEAD activity and
163 persistent activation of YAP abolishing contact inhibition of proliferation.
164
165 **YAP-regulated cell cycle entry and exit is dictated by a cyclin D1/p27 threshold**
166 We next used the quantitative analysis of the balance between contact inhibition and mitogen
167 signaling to identify the mechanism of how YAP regulation controls cell-cycle entry and exit.
168 Cells enter the cell cycle during the G1 phase by activating cyclin-CDK complexes to
169 hyperphosphorylate Rb and derepress the E2F cell cycle transcription program[25]. In contrast, in
170 cells that exit the cell cycle or stay arrested, cyclin-CDKs stay inactive and Rb remains
171 dephosphorylated. In monolayers of RPE1 and other epithelial cells, this bimodal Rb
172 phosphorylation is thought to be primarily controlled by the CDK4/6 activator cyclin D1 and the
173 cyclin-CDK2/4/6 inhibitor p27[22], and cyclin D1 is generally thought to contribute to the YAP-
174 mediated proliferation regulation[3]. We included p27 in our analysis since both cyclin D1[31] and
175 p27 are key regulators of cell proliferation in vivo, with p27 deletion resulting in multi-organ
176 hyperplasia[32].
177 Using multiplexed immunofluorescence[33], we computationally gated for G1 cells by their
178 diploid 2N DNA content and lack of incorporation of EdU (Figure S2A). We then measured the
179 levels of nuclear localized cyclin D1 and p27 and whether Rb was phosphorylated in each G1-
180 phase cell. Notably, p27 protein levels are often used as a marker of non-proliferating cells, but
181 we observed substantial heterogeneity in the nuclear levels of both p27 and cyclin D1 across
182 individual cells irrespective of Rb phosphorylation (Figure S2B). Increasing the mitogen stimulus
183 (from 0.1% to 10% serum) resulted in the cell population shifting towards higher average cyclin
184 D1 levels and lower average p27 levels.
185 We next determined how local cell density and YAP activity regulate the cyclin D1 and
186 p27 levels. As local density increased, the median cyclin D1 level of WT cells gradually
187 decreased, while the median p27 level strongly increased (Figure 2A). This trend was opposite
188 to the effects of increasing serum, which both globally increased cyclin D1 levels and
189 suppressed the density-dependent increase in p27 protein. Markedly, the CA-YAP cells lost the
190 serum and density dependence of both, keeping the levels of cyclin D1 high and p27 low in G1
191 phase, arguing that YAP activity is not only upregulating the level of cyclin D1 but also
192 downregulating the level of p27 (Figure 2B).

193 Explaining why the level of cyclin D1 or p27 alone cannot predict whether Rb is
194 phosphorylated, only the level of cyclin D1 relative to p27 was tightly correlated with Rb
195 phosphorylation in individual cells. Only cells with relatively more cyclin D1 than p27 had Rb
196 phosphorylated (Figure 2C-D, S2C). Thus, even for low mitogen levels, a small fraction of cells
197 had sufficiently high cyclin D1 and low p27 to have Rb phosphorylated. Conversely, at high
198 mitogen stimulation, more cells populated the high-cyclin D1/low-p27 state and had Rb
199 phosphorylated, demonstrating a critical threshold cyclin D1/p27 ratio for proliferation.
200 Strikingly, in CA-YAP cells with persistently active YAP, Rb phosphorylation remained
201 closely predicted by the relative nuclear cyclin D1 and p27 levels (Figure 2E, S2D-E), implying
202 that YAP is signaling through both cyclin D1 and p27 to control proliferation. Notably, we
203 identified some CA-YAP cells with high cyclin D1 that did not have Rb phosphorylated, but
204 these cells had increased protein levels of another CDK inhibitor, p21, which we demonstrated
205 in separate experiments (Figure 2F). Since p21 levels were only weakly regulated by serum
206 starvation or contact inhibition (Figure S2F-G), p27 is functioning as the primary proliferation
207 suppressor relevant for contact inhibition and YAP signaling[34,35].
208 The fundamental role of the cyclin D1/p27 ratio in YAP-regulated proliferation is further
209 seen in a comparison of different perturbations that change the cyclin D1/p27 ratio and
210 correspondingly change Rb phosphorylation (Figure 2G). The siRNA-mediated knockdown of
211 cyclin D1 strongly reduced the proportion of cells with phosphorylated Rb by shifting most of the
212 CA-YAP cells to a high-p27 and quiescent state, but again preserved the control of Rb
213 phosphorylation by the cyclin D1/p27 ratio (Figure 2H, S2H). Moreover, knocking down p27 in
214 WT cells resulted in more cells ending up below the dashed line but still preserved the control of
215 Rb phosphorylation by the cyclin D1/p27 ratio (Figure 2G). Conversely, in cells where p27 levels
216 were increased by CRISPRa induction, most cells were above the dashed line and proliferation
217 was completely suppressed (Figure 2I). However, LATS inhibitor-mediated activation of YAP in
218 these cells lowered p27 and increased cyclin D1 to push some cells below the threshold cyclin
219 D1/p27 ratio where they could again proliferate (Figure 2I).
220 We conclude that the crucial parameter for the YAP-regulated control of cell cycle entry
221 is the nuclear cyclin D1/p27 ratio in G1 phase, with a threshold dictating whether individual cells
222 enter or exit the cell cycle (Figure 2J). Moreover, YAP activity and mitogen signaling both
223 control proliferation through the same downstream cyclin D1/p27 ratio. Notably, we were only
224 able to identify this molecular mechanism of how YAP controls the cell cycle entry and exit
225 decision by measuring nuclear p27, cyclin D1 and p-Rb levels within the same, G1-gated single
226 cell.

227

228 **YAP regulation gradually changes the nuclear cyclin D1/p27 ratio**

229 We next used RNA sequencing (RNAseq) to distinguish between different potential signaling
230 pathways through which YAP activation may regulate cyclin D1 and p27 levels over time.
231 Previous studies suggested various regulatory mechanisms, such as direct induction of cyclin
232 D1[14], indirect induction of mitogen signaling, or reprogramming the cell state[15,36,37]. We
233 measured gene expression changes up to 36-hours following CA-YAP induction in low serum
234 cells (Figure 3A). Critically, we inhibited CDK4/6 activity in these cells (palbociclib) to keep cells
235 in a state with minimal E2F activation to suppress the otherwise dominating effects of the E2F
236 cell cycle transcription program that may obscure the YAP-specific transcription program.

237 We confirmed that the conserved YAP target gene signature[38] was significantly enriched
238 after 12-36 hours of induction (Figure 3B), including the canonical YAP target genes *CYR61* and
239 *ANKRD1* that were significantly induced within 6h (Figure 3C, S3B). We also confirmed
240 previously-characterized induction of G1-related target genes *CDK6*[39] and *SKP2*[40] (Figure S3B),
241 proliferation-supporting transcription factors (*MYBL1, ETS1, MYC,* Figure S3C)[15], as well as
242 TEAD and AP1 target genes[18] (*TEAD1/2*, *FOSL1/2, JUN*, Figure S3D). Compared with the fast
243 induction of the YAP target gene *CYR61*, we observed *CCND1* (cyclin D1) expression
244 increasing only after 12-36 hours and only 1.4-fold. In comparison, the previously-reported
245 suppressed gene *DDIT4*[41] rapidly dropped whereas the expression of p27 (*CDKN1B*) and p21
246 (*CDKN1A*) changed only minimally over time (Figure 3D).

247 Since there was only a small fold change in cyclin D1 and p27 expression, we next
248 tested whether cyclin D1 and p27 are more strongly regulated at the protein level[42–44] following
249 acute YAP-TEAD activation. LATS inhibitor treatment of serum-starved WT cells increased the
250 nuclear/cytoplasmic YAP ratio and we confirmed the protein-level increase of select YAP targets
251 (CDK6 and SKP2, Figure S3E). LATS inhibition strongly increased cyclin D1 protein levels but
252 also resulted in a small increase in p27 and transient decrease in p21 (Figure 3E, S3F). Over 3-
253 12 hours following LATS stimulation, the increase in the cyclin D1/p27 ratio was paralleled by
254 increasing Rb phosphorylation (Figure 3F-G), and cells progressed to S-phase within 12-24
255 hours (Figure S3G). Supporting that LATS signals through YAP-TEADs, TEAD inhibition
256 reversed the LATSi-induced changes of these protein levels and reversed the percent of
257 proliferating cells back to control levels (Figure 3F, S3G).

258 We next inhibited TEAD in proliferating cells to determine how YAP-TEAD inhibition
259 regulates cyclin D1 and p27 levels and Rb phosphorylation in G1 phase to terminate
260 proliferation. We first confirmed that TEAD inhibition of CA-YAP cells, or of LATSi pre-treated

261 WT cells, rapidly reduced the YAP ratio (Figure S3H). Markedly, however, TEAD inhibition
262 resulted in only a delayed reduction of the nuclear level of cyclin D1 protein in G1 phase (Figure
263 3H). Moreover, TEAD inhibition caused a strong and slow increase of the nuclear protein levels
264 of p27 and a relatively smaller increase in p21 levels across the population. Concordantly, the
265 mean cyclin D1/p27 ratio and the G1 phase Rb phosphorylation both decreased but only after a
266 delay with most cells arresting by 24-36 hours (Figure 3I, S3I). Moreover, single-cell analysis
267 confirmed that the cyclin D1/p27 ratio still predicted whether Rb was phosphorylated in G1 as
268 individual cells gradually reduced their cyclin D1 and increased their p27 level (Figure 3J).
269 Thus, while acute YAP activation increases the cyclin D1/p27 ratio and triggers Rb
270 phosphorylation relatively quickly, YAP inactivation in proliferating cells lowers the cyclin D1/p27
271 ratio and Rb phosphorylation only after a delay of 12 to 24 hours. This result raises the question
272 of how YAP activity can induce such a prolonged increase in the cyclin D1/p27 ratio that keeps
273 Rb hyperphosphorylated in G1-phase cells long after YAP has been inhibited.
274
275 **YAP activation induces and prolongs proliferation by increasing EGFR signaling**
276 Our RNAseq time course analysis also supported earlier data that YAP activation increases
277 multiple factors related to receptor signaling[16,45–47] (Figure 4A, S4A). These factors included
278 receptors and secreted ligands known to regulate cell proliferation including *ERBB3* and *AXL*
279 receptors[3], along with ligands like *FGF1/2* and the EGFR ligand precursor *HBEGF* (paralog of
280 *AREG*)[48,49], providing a potential cell autonomous activation of EGFR and other receptors. We
281 were intrigued by this possibility since the slow kinetics of the expression changes matched the
282 delay we observed in the changes of the cyclin D1/p27 ratio in the G1 phase after TEAD
283 inhibition.
284 Since expression levels of *AXL* (a direct YAP target gene)[15,50,51], *EGFR,* and *HRAS* were
285 all gradually increased by YAP activation, along with the EGFR-activating ligand *HBEGF* (Figure
286 4B), we first considered whether the residual proliferation observed in serum starved cells might
287 be induced by YAP through activation of EGFR signaling. Indeed, the small portion of WT cells
288 proliferated in the absence of mitogens could be inhibited by titration of the EGFR inhibitor
289 gefitinib in the absence of exogenous EGF (Figure 4C). The EGFR inhibition also mirrored the
290 TEAD inhibition, supporting that YAP-TEAD activity may signal through EGFR at low stimulation
291 conditions to promote proliferation (Figure S1G). However, EGFR inhibition in CA-YAP cells
292 could only partially suppress Rb phosphorylation (Figure 4E, Figure S4B), suggesting that
293 additional receptor signaling pathways are contributing to the YAP-induced proliferation.

294 We next determined how rapidly TEAD inhibition changes the protein level of EGFR and
295 AXL. Western blot analysis revealed that their total levels gradually decreased after TEAD
296 inhibition in CA-YAP cells over a similar time scale as the loss of proliferation (Figure 4D). Since
297 EGFR levels were YAP dependent, we further tested whether YAP activation increases EGF
298 sensitivity. Indeed, while EGF stimulation caused only a small increase in Rb phosphorylation in
299 WT cells, Rb phosphorylation was much more strongly increased in CA-YAP cells (Figure 4E).
300 Furthermore, while both WT and CA-YAP cells had similarly low basal AKT and ERK
301 phosphorylation, the CA-YAP cells kept their phosphorylated AKT and ERK levels higher for at
302 least 10 hours after EGF stimulation compared to WT cells, again consistent with sensitized
303 EGF signaling (Figure 4F). As a control, we also confirmed that TEAD inhibition of CA-YAP cells
304 prevented this prolonged AKT and ERK signaling.
305 Finally, we tested whether there is an extended period of enhanced EGF signaling also
306 after transient LATS inactivation upstream of YAP. We used WT cells pre-treated with LATSi
307 and then either maintained (sustained) or washed out the LATSi prior to a 14-hour addition of
308 EGF (Figure 4G). While LATSi washout reduced the nuclear/cytoplasmic YAP ratio and nuclear
309 YAP levels back to control conditions (Figure 4G, S4C), cells retained sensitivity to EGF for at
310 least 14 hours, as evidenced by the increased p-Rb (Figure 4H, Figure S4D), S6
311 phosphorylation (p-S6, a readout of PI3K/mTOR activity, Figure 4I, S4E), and nuclear FRA1
312 levels (a readout of integrated MEK-ERK activity[52], Figure 4J). In support of a general
313 prolongation of proliferation signaling, we also found that transient LATSi treatment sustained
314 the fraction of G1 cells with phosphorylated Rb after HGF and LPA stimulation (Figure S4F).
315 We conclude that YAP activity increases the activity of EGFR in the absence of added
316 EGF in an autocrine manner[16,48], while also increasing the sensitivity of cells to exogenous EGF
317 stimulation. This sensitization extends to other receptors since gefitinib could only suppress a
318 fraction of the YAP-induced proliferation response. Notably, the increased EGFR signaling
319 persisted for over 14 hours after YAP inactivation, suggesting that YAP is inducing a prolonged
320 proliferation response since YAP inactivation only terminates proliferation and signaling after a
321 delay.
322
323 **YAP activation signals primarily through MEK-ERK to increase the cyclin D1/p27 ratio**
324 We next examined which signaling pathways downstream of the YAP-induced receptor
325 activation control the cyclin D1/p27 ratio. We focused on PI3K-AKT-mTOR and MEK-ERK
326 signaling[45,53], since various functions of YAP activation are mediated through mTOR
327 activation,[54,55] and both mTOR and MEK-ERK can regulate cyclin D1 and p27 levels[20,34,56]

328 (Figure 5A). We measured phosphorylation of AKT and S6 protein (p-S6) to monitor PI3K
329 pathway activity and protein levels of the transcription factor Fra1 to monitor the ERK pathway.
330 Serum-starved CA-YAP cells displayed both elevated p-AKT(S473) and p-S6(240/244) as well
331 as Fra1 levels (Figure 5B-C), which similarly depended on YAP-TEAD activity, as TEAD
332 inhibition reduced their phosphorylation and protein levels in CA-YAP cells (Figure 5D).
333 To assess the functional importance of PI3K-AKT-mTOR signaling, we inhibited PI3K
334 (LY-294002) or AKT (MK2206), which had only small inhibitory effects on Rb phosphorylation in
335 CA-YAP cells (Figure 5E), despite reducing the p-AKT(S473) and p-S6(240/244 and 235/236)
336 levels (Figure S5A-B). Nevertheless, inhibiting mTORC1/2 (mTORi, Torin2) caused an
337 approximately 50% reduction in proliferation (Figure 5E). In contrast, inhibition of the obligate
338 upstream regulator of ERK, MEK (MEKi, PD0325901), completely suppressed Rb
339 phosphorylation and readouts of ERK activity (Figure 5F, S5C-D).
340 In support of YAP regulating cyclin D1 protein levels in G1 phase through mTOR and
341 MEK/ERK, rather than doing so directly, MEK inhibitor alone (Figure S5D) or the combined
342 inhibition of MEK and mTOR fully reduced the cyclin D1 level in CA-YAP cells to the level of WT
343 cells (Figure 5G, S5E). A time course analysis showed that the drop in cyclin D1 levels is rapid
344 after mTOR inhibition but slower and stronger after MEK inhibition even though both inhibitors
345 rapidly suppressed p-S6 and p-ERK, respectively (Figure 5H-I). As mTOR can rapidly control
346 translation of cyclin D1 mRNA[57], this fast regulation was anticipated. In contrast, mTOR
347 inhibition did not alter p27 levels but MEK inhibition not only reduced cyclin D1 levels but also
348 slowly and strongly increased p27 levels, explaining why MEK inhibition suppresses Rb
349 phosphorylation more completely than the regulation of mTOR. Thus, transient YAP-mediated
350 proliferation responses result from an increase and delayed decrease of the activity of EGFR
351 and other receptors, which in turn transiently increases the cyclin D1/p27 ratio through
352 reversibly regulating MEK-ERK and, to a lesser degree, mTOR signaling pathways.
353
354 **Partial activation of YAP from ablating Merlin can be reversed by increased contact**
355 **inhibition**
356 To evaluate the robustness of the termination of YAP activation in monolayers, we increased
357 YAP activity by ablating Merlin, an adaptor protein and tumor suppressor that indirectly activates
358 LATS1/2[58–60]. We generated clonal Merlin knockout RPE1 cells (Merlin KO) using
359 CRISPR/Cas9. As expected, these cells had increased nuclear localization of YAP that could be
360 suppressed by TEAD inhibition (Figure S6A-B).

361 However, unlike CA-YAP, Merlin KO increased proliferation without abolishing contact
362 inhibition of proliferation. Instead, a higher cell density was required to inhibit proliferation
363 compared to WT, both at low and high serum levels (Figure 6A, S6C). Moreover, inhibiting
364 TEAD in Merlin KO cell suppressed Rb phosphorylation in both cases to levels similar as TEAD-
365 inhibited WT cells (Figure S1G), supporting a model whereby Merlin regulates proliferation
366 primarily through YAP-TEAD activity[9]. Importantly, we found that YAP activity in Merlin KO cells
367 could be as effectively inhibited by contact inhibition as in WT cells but required a higher local
368 cell density to reach the same YAP inhibition (both at low and high serum levels, Figure 6B).
369 We next examined the role of EGFR in the Merlin KO cells, as a possible mechanism
370 mediating serum-independent proliferation downstream of the higher YAP signaling. Like CA-
371 YAP cells, Merlin KO cells displayed activated EGFR signaling in the absence of added EGF,
372 since the EGFR inhibitor gefitinib reduced the percentage of proliferating cells (Figure 6C, S6D).
373 Similar to the transiently LATS-inhibited cells, the Merlin KO cells had increased sensitivity to
374 EGF while still retaining a strong local cell density dependence (Figure 6E). In addition, we
375 found increased proliferation in response to several other receptor tyrosine kinase ligands
376 (Figure S6D), again consistent with YAP inducing a broad upregulation of receptor signals not
377 limited to EGFR.
378 Finally, we found that Merlin KO cells still suppressed cyclin D1 and increased p27
379 levels at higher local cell density (Figure 6E), demonstrating that these cells suppress
380 proliferation through the same mechanism as WT cells: inhibiting YAP activity and
381 downregulating mitogen signaling and the cyclin D1/p27 ratio (Figure 6F). However, Merlin KO
382 cells employ alternative mechanisms from inactivating Merlin[61,62] to contact inhibit YAP.
383 We conclude that even though constitutive YAP activation abolished contact inhibition of
384 proliferation, cells can robustly contact inhibit YAP-TEAD even if Hippo signaling is reduced and
385 YAP activation increased. However, cells that have such an induced YAP activity now require
386 higher local cell density to suppress YAP activity and proliferation.
387
388 **DISCUSSION**
389 Our study shows that contact inhibition of YAP and mitogen signaling control the cyclin D1/p27
390 ratio and cell cycle entry in G1 phase through a balance mechanism that shapes an intrinsically
391 transient YAP-induced proliferation response (Figure 6G). Our study supports a model where
392 YAP activation controls proliferation by gradually increasing the expression of HB-EGF and
393 other RTK ligands, as well as various receptors and known regulators of mitogen signaling[3,54,63].
394 This regulation explains how YAP activation is increasing EGF and other mitogen signals in a

395 cell autonomous manner (Figure 4C), while simultaneously sensitizing cells to exogenous
396 stimulation by EGF and other mitogens (Figure S4F, S6E), which is likely relevant for the role of
397 YAP activation in the inflammatory injury response[64,65]. We further show that YAP activation
398 increases downstream signaling through MEK-ERK signaling and, to an unexpectedly lesser
399 degree, mTOR signaling, to control the nuclear protein levels of cyclin D1 and p27 (Figure 5I).
400 Most importantly, our study revealed a predominant role of both cyclin D1 and p27 in YAP-
401 induced proliferation. We showed that YAP-stimulated cells decide in the G1 phase whether to
402 enter the cell cycle by increasing the nuclear cyclin D1/p27 ratio above a critical activity
403 threshold, or to remain quiescent or exit the cell cycle by staying below this threshold (Figure
404 2C-E).
405 Moreover, as the YAP-induced cell division increases the local cell density, we show that
406 the ensuing contact inhibition of YAP-TEAD causes a delayed inhibition of mitogen signaling,
407 which lowers the cyclin D1/p27 ratio to terminate the proliferation response. Thus, there are two
408 delay mechanisms ensuring a prolonged proliferation response: cells wait to inhibit YAP until
409 cell division has increased the local cell density, then the resulting contact inhibition of YAP
410 lowers the cyclin D1/p27 ratio and arrests proliferation after a delay (Figure 6H). YAP signals
411 often fluctuate[66–68], and the slow integration of YAP signals further ensures that the proliferation
412 response is robustly started and ended. Slow integration provides a filter mechanism which
413 prevents short-lived YAP activity changes from triggering unwanted cell cycle entry or
414 premature cell cycle exit.
415 We also evaluated the robustness of YAP inactivation by using ablation of Merlin/NF2, a
416 suppressor of Hippo signaling to YAP[69–71]. While Merlin has been shown to have additional
417 signaling functions at the plasma membrane, our study shows that the increased EGFR
418 signaling and proliferation in Merlin KO cells can be reversed by TEAD inhibition (Figure 6A),
419 suggesting that Merlin primarily signals through YAP-TEAD to control EGFR signaling, the
420 cyclin D1/p27 ratio, and proliferation. In support that the termination of YAP signaling and
421 proliferation is robust, our study shows that contact inhibition is merely shifted but not abolished
422 when YAP activity is increased by ablation of Merlin, and cells can still effectively terminate
423 proliferation but at higher local cell density. Moreover, since the loss of Merlin can boost
424 proliferation without a loss of contact inhibition, this result also suggests that Merlin has a
425 unique advantage as a drug target, since a potential Merlin inhibitor would trigger a self-limiting
426 proliferation response. This could offer a safer alternative strategy to LATS inhibition, which was
427 recently shown to cause a widespread and uncontrolled proliferation response and de-
428 differentiation in mice[6].

429 We also found that inhibiting MEK-ERK, rather than mTOR, in CA-YAP cells greatly
430 reduces the cyclin D/p27 ratio and stops proliferation. This crucial role of MEK-ERK in YAP-
431 induced proliferation was surprising, since oncogenic YAP mutants can drive resistance to
432 KRAS inhibition and KRAS primarily regulates proliferation through MEK-ERK and mTOR
433 activation[29,45,72]. The resistance to KRAS inhibitor may therefore by mediated by YAP-mediated
434 direct regulation of cell cycle entry. We confirmed that YAP activation can also directly induce
435 cyclin D1 as well as SKP2, which can degrade p27[73,74]. Indeed, we found that this upregulation
436 may be particularly important at high levels of YAP activation[75,76], since DOX induction of CA-
437 YAP in high serum conditions can still increase cyclin D1 and proliferation when MEK is
438 inhibited (Figure S6F-G).
439 Our study also supports that YAP regulates proliferation through additional modulatory
440 pathways described in previous studies. YAP gradually induces a number of Hippo pathway
441 components such as LATS, Merlin and Angiomotin-like genes[77,78] (Figure S6H-I), which likely
442 contribute to the delayed downregulation of YAP along with the contact inhibition of YAP.
443 Moreover, our finding that persistent activation of YAP suppresses contact inhibition of
444 proliferation is supported by our own and previous RNAseq data[15,19] showing that YAP
445 activation not only increases mitogen signaling regulators but also reduces the expression of
446 contact inhibition regulators at the plasma membrane such as ephrins[49] and protocadherins[79,80]
447 (Figure S6J-K), which may mediate cell density sensing. Finally, we showed the stress-
448 regulated p21 CDK inhibitor can be rate-limiting in suppressing proliferation in some YAP-
449 activated cells (Figure 2F), supporting a redundant role of both p27 and p21 inhibitors in
450 promoting cell cycle exit.
451
452 **Concluding remarks**
453 YAP activation must be transient to drive the epithelial regenerative response. Our study
454 identifies a self-limiting control mechanism that allows YAP to trigger a commensurate
455 proliferation response. We show that transient proliferation responses are initiated by YAP
456 activation increasing EGF and mitogen signaling to increase the cyclin D1/p27 ratio above a
457 critical threshold. The delayed contact inhibition-mediated inactivation of YAP then terminates
458 proliferation by gradually lowering mitogen signaling and the cyclin D1/p27 ratio below this
459 critical threshold (Figure 6H). In contrast, we demonstrate that persistent inactivation of
460 LATS1/2 or activation of YAP activity abolishes contact inhibition and promotes persistent
461 mitogen signaling that keeps the cyclin D1/p27 ratio high, explaining how oncogenic mutations
462 that constitutively inactivate LATS1/2 or activate YAP elicit unrestricted proliferation.

463

464 **Limitations**

465 We identified cyclin D1 and p27 as the primary regulators of Rb phosphorylation for RPE1 cells
466 in response to contact inhibition and serum starvation with an added contribution from p21. In
467 other cell types and cancer models, additional phosphorylation, degradation, and translation-
468 mediated control steps may further contribute to the timing and overall level of proliferation. We
469 also studied EGFR signaling as a representative effector of YAP, but our data suggest a
470 pleiotropic effect on additional receptors and cell adhesion pathways, which likely affect the
471 activity of Merlin and other adaptor proteins at the plasma membrane and feed into the
472 dynamics of different mitogen responses. Furthermore, as our mechanistic studies required in
473 vitro*,* single-cell experiments, how these control mechanisms of the proliferation response apply
474 to various animal models of epithelial repair remains to be determined. Finally, in addition to
475 Merlin, other adaptor proteins like angiomotin and cytoskeleton regulators like RhoA, can
476 regulate YAP activity in response to cell density changes. Future work is also needed to
477 understand specific contributions from such regulators and when they engage to restrict or
478 promote YAP-TEAD activity.

479

480 **Acknowledgments**

481 We thank Nathaniel Kastan and James Hudspeth for early access to a previous iteration of the
482 LATS1/2 inhibitor (TRULI); Alexander Pfannenstein, Marielle Koeberlin, and Sanjeev Sharma
483 for technical support; the Stanford Shared FACS Facility and Weill Cornell FACS Facility for cell
484 sorting; the Weill Cornell Genomics Core for library prep and RNA-sequencing; Marielle
485 Koeberlin for critical reading of the manuscript; and James Ferrell, Alexander Dunn, Daniel
486 Jarosz, Ovijit Chaudhuri, Elizabeth Kiddie, Members of the Meyer and Teruel laboratories for
487 technical feedback and helpful discussions. This work was funded by an NIH T32 training grant
488 (5 T32 GM 113854-3), NIH grants T.M. (R35 GM12702601) and M.N.T. (R01 DK131432); K.F.
489 was supported by an NSF Graduate Research Fellowship (DGE-1656518).

490

491 **Author contributions**

492 Conceptualization, K.F., Y.F., and T.M.; Methodology, K.F., N.R., Y.F., and T.M.; Experiments,
493 visualization, and analysis, K.F.; Manuscript preparation, K.F., M.N.T., and T.M.; Funding
494 acquisition, T.M., and M.N.T.

495

496 **Declaration of interests**

497 The authors declare no competing interests.
498
499 **Resource availability**
500 Immunofluorescence protocols, and cell lines are available upon request to the lead contact.
501 Plasmids generated in this study will be deposited to Addgene.
502
503 **Data and code availability**
504 MATLAB image-processing scripts and iterative imaging analysis pipeline are previously
505 published[22,81] and publicly available on Github (https://github.com/MeyerLab/image-analysis-
506 ratnayeke-2022).
507 Additional information is available upon request from the lead contact.
508
509 **Supplemental information titles and legends**
510 Figures S1-S7 and Tables S1-S2
511
512 **STAR METHODS**
513 **Cell culture**
514 All experiments were performed with human retinal pigmented epithelial cells (RPE1-hTERT
515 immortalized, ATCC Cat# CRL-4000) unless specified otherwise. RPE1 were cultured in
516 DMEM/F12 growth media with HEPES (Thermo Scientific Cat#11039047), supplemented with
517 10% fetal bovine serum (Millipore Sigma Cat#F4135-500ML) and passaged using trypsin-EDTA
518 (0.05%, Gibco Cat# 25300054). Human mammary epithelial cells (MCF10A, ATCC Cat# CRL-
519 10317, RRID:CVCL_0598) were cultured in DMEM/F12 growth media with HEPES
520 supplemented with 5% horse serum (Gibco Cat# 16050122), 20 ng/mL EGF (PeproTech Cat#
521 C8052), 0.5 µg/mL hydrocortisone (Sigma Cat#H0888), 100 ng/mL cholera toxin (Sigma Cat#
522 C8052), and 10 µg/mL insulin (Sigma Cat#I1882). For serum starvation experiments, cells were
523 first washed with serum-free DMEM/F12 media, then maintained in serum-free (0%) or 0.1%
524 serum-containing DMEM/F12 (serum-starvation conditions). 0.1% serum-containing media had
525 similar proliferation as 0% serum-containing media, but cells were slightly more adherent to
526 glass-bottom plates for subsequent immunofluorescence protocols and therefore used for a
527 subset of experiments. For mitogen-release experiments, mitogens and growth factors (EGF,
528 HGF, and FGF at 25 ng/mL and LPA at 1 µM) were diluted in starvation media. HEK-293T cells
529 used for lentivirus production were cultured in DMEM growth media (Gibco Cat# 11995065)
530 supplemented with 10% fetal bovine serum. Cells were cultured at 37 °C and 5% CO2.

531

532 **Plasmid generation**

533 pSpCas9(BB)-2A-Puro (PX459) V2.0 was a gift from Feng Zhang (Addgene # 62988,
534 RRID:Addgene_62988). Phosphorylated and annealed sgRNA oligos against *NF2* (see Cell line
535 generation below) were cloned into restriction enzyme-digested PX459[82].

536 pQCXIH-Myc-YAP-5SA was a gift from Kun-Liang Guan (Addgene #33093, RRID:
537 Addgene_33093). Doxycycline-inducible, myc-epitope-tagged CA-YAP (YAP5SA) was
538 generated using Gibson assembly of PCR-amplified myc-YAP5SA with restriction enzyme-
539 digested plasmid backbone derived from a bicistronic vector with a TetOn promoter driving
540 target gene expression and PGK-driven rtTA expression, pCW-Cas9 (Addgene #50661, RRID:
541 Addgene_50661, a gift from Eric Lander and David Sabatini).

542

543 **Cell line generation**

544 Merlin knockout cells were generated by transient transfection of parental RPE1 cells with
545 pX459 (2 ng/uL, containing gRNA scaffolds targeting Merlin/Nf2) and Lipofectamine 2000
546 (1:500, Thermo Cat# 11668019) in Opti-MEM (Fisher Scientific Cat#31-985-070) and growth
547 media overnight, then exchanged for growth media with puromycin selection (10 µg/mL,
548 Invivogen Cat#ant-pr-1) for 72h. After a recovery period in selection-free media, cells were
549 diluted to 0.5 cells/100 µL and seeded to 96-well plates for single-cell clonal expansion. 24
550 single-cell clones were further expanded for preliminary knockout assessment by western blot
551 for loss of Merlin protein expression. 2 clones (Merlin KO-clone 1 forward:
552 CACCGCACAGTGGCCTGGCTCAAAA, reverse: AAACTTTTGAGCCAGGCCACTGTGC ;
553 Merlin KO-clone 2 forward: CACCGTGATTTGGTGTGCCGGACTC, reverse:
554 AAACGAGTCCGGCACACCAAATCAC) were selected for validation by genomic DNA
555 purification (Qiagen CAT#69504), PCR of the Merlin locus and sequencing. After initial
556 characterizations confirming Merlin KO-clone 1 and Merlin KO-clone 2 were similarly
557 proliferative (data not shown), we proceeded to use KO-clone 1 for all subsequent experiments
558 in this study.

559 Lenti-EF1a-dCas9-VPR-Puro (Addgene # 99373, RRID: Addgene_99373) was a gift
560 from Kristen Brennard and stably expressed in RPE1 cells using puromycin selection (10
561 ug/mL, Invivogen Cat#ant-pr-1). CA-YAP and dCas9-expressing cells were generated using
562 third-generation lentiviral transduction. Lentivirus was generated in HEK-293T cells by
563 transfection with packaging and envelope plasmids pMDLg/pRRE (Addgene # 12251, RRID:
564 Addgene_12251), pRSV-rev (Addgene #1225, RRID: Addgene_1225), and pCMV-VSV-G

565 (Addgene #8454, RRID: Addgene_8454) in Lipofectamine 2000 and Opti-MEM. After 72h
566 transfection, supernatant was passed through a 0.22 uM filter (Millipore Cat# SCGP00525) and
567 concentrated using 100 kDa centrifugal filters (Millipore Cat# UFC910024). Lentivirus was then
568 frozen or directly transduced into cells. 72h after lentiviral transduction, cells were split into
569 antibiotic-selection media or, if expressing a fluorescent construct, expanded prior to sorting by
570 a BD Influx cell sorter (Stanford Shared FACS Facility, Weill Cornell FACS Facility).
571
572 **siRNA, sgRNA, and plasmid transfection**
573 All oligo sequences are listed in Table S1. Pooled siRNA (ON-TARGETplus, Horizon Discovery
574 Biosci.) were used for siCtrl (Non-targeting Control, Horizon Cat#D-001810-10-05), siCycD1
575 (siCCND1, Horizon Cat# L-003210-00-0005), and sip27 (siCDKN1B, Horizon Cat# L-040178-
576 00-0005). For CRISPRa-mediated overexpression of genes through targeting of endogenous
577 promoters, pooled sgRNA (Horizon) were used for sgCtrl (non-targeting control, Horizon Cat#
578 U-009500-10-05), sgCycD1 (sgCCND1, Horizon Cat# P-003210-01-0005), and sgp27
579 (sgCDKN1B, Horizon Cat# P-003472-01-0005) with tracRNA (Edit-R tracrRNA, Cat# U-002005-
580 05). RPE1 cells were transfected with siRNA and sgRNA using DharmaFECT 1 (1:500 in Opti-
581 MEM, Dharmacon Cat# T-2001-03) according to manufacturer protocol using 20 nM siRNA, or
582 sgRNA and tracrRNA (in 1:1 ratio, according to manufacturer protocol). Cells were incubated in
583 transfection mixture for 6-12h in growth media, then replaced with media appropriate for the
584 experiment conditions and assessed 24-48h after transfection.
585
586 **Drugs and mitogens**
587 Human growth factors and mitogens were dissolved in sterile, ultrapure water (Fisher Scientific
588 Cat#10977023) and used at the following concentrations unless otherwise stated: 25 ng/mL
589 recombinant EGF (PeproTech cat#AF-100-15), 25 ng/mL recombinant HGF (Life Technologies
590 Cat#PHG0254), 25 ng/mL recombinant FGF basic (R&D Systems Cat#233-FB-025), 1 uM LPA
591 (oleoyl-L-alpha-lysophosphatidic acid, Sigma-Aldrich Cat#L7260-1MG).
592 Drugs were dissolved in DMSO (Sigma-Aldrich Cat# D2650) and used at the following
593 concentrations unless otherwise stated: 0.5 μM TDI-011536 (Selleck Chemicals Cat#E1314,
594 CAS#2687970-96-1, LATSi), 5 μM TRULI (a gift from James Hudspeth, CAS#1424635-83-5), 1
595 μM GNE-7887 (ChemieTek Cat#CT-GNE7883, CAS# 2648450-42-2,TEADi), 10 μM gefitinib
596 (Selleck Chemicals Cat#S1025, CAS#184475-35-2, EGFRi), 10 μM LY294002 (Cayman
597 Chemical Cat#70920, CAS#154447-36-6 , PI3Ki), 200 nM MK2206 (Cayman Chemical
598 Cat#11593, CAS#1032350-13-2, AKTi), 100 nM Torin2 (Cayman Chemical Cat#14185,

599 CAS#1223001-51-1, mTORi), 100 nM PD0325901 (Selleck Chemicals Cat#S1036,
600 CAS#391210-10-9, MEKi), 1 μM palbociclib (PD-0332991, Selleck Chemicals cat#S1116,
601 CAS#827022-32-2, CDK4/6i), 0.5 ug/mL doxycycline hyclate (Sigma-Aldrich cat#D9891,
602 CAS#24390-14-5, DOX), 10 μM 5-ethynyl-2'-deoxyuridine (EdU, Cayman Chemical Cat#20518,
603 CAS# 61135-33-9). For drug treatments and time courses, control conditions were treated with
604 DMSO, except mitogen release controls (mock), which were dissolved in water. For all EdU-
605 incorporation, cells received an EdU spike-in (10 μM, in serum-free media) for 12-15 min prior to
606 fixation.
607
608 **Western blotting**
609 Cells grown in 6-well plates were washed once in cold, sterile PBS and lysed in chilled, 1x RIPA
610 buffer (Boston BioProducts Cat#BP-115-5X) or non-denaturing lysis buffer (20 mM HEPES, 150
611 mM NaCl, 2 mM EDTA, 0.1% IGEPAL-CA630) containing HALT protease and phosphatase
612 inhibitor cocktail (1:100, Thermo Fisher Cat#78439). Lysates were harvested on ice using cell
613 scrapers, sheared by syringe (25G) and centrifuged at 15,000 RCF for 15 min at 4C.
614 Supernatant was stored at -20C. Protein concentration was calculated by Pierce BCA Protein
615 Assay (Thermo Fisher Cat#23225) according to manufacturer protocol and a BSA standard
616 curve.
617 10-30 ug protein was loaded onto 7.5%, 12%, or 4-20% Mini-PROTEAN TGX gels for
618 resolution by SDS-PAGE in 1x Laemmli sample buffer (Fisher Scientific, Cat#AAJ60660AC, or
619 Bio-Rad Cat#1610737) alongside Page RulerPlus (Thermo Scientific Cat#26620) molecular
620 ladders in Tris/Glycine/SDS running buffer (Bio-Rad Cat#161-0772). Gels were run at 150V for
621 1h then transferred to 0.2 um PVDF membranes by semi-dry transfer (Bio-Rad Trans-Blot SD,
622 Cat# 1703940) in Tris/Glycine buffer (Bio-Rad Cat# 1610734) with 10% methanol, or semi-dry
623 transfer (Bio-Rad Trans-Blot Turbo Cat# 1704150) with Trans-Blot Turbo Transfer Packs (Bio-
624 Rad Cat# 1704156). Membranes were washed in TBST (20 mM Tris, pH 7.5, 150 mM NaCl,
625 0.1% Tween-20), blocked for 30 min in 5% milk/TBST (VWR Cat#10128-602), and incubated at
626 RT for 3h or overnight at 4C in primary antibody dilutions in 5% BSA/TBST + 0.01% NaN3.
627 Primary antibodies used were rabbit anti-AXL (1:1000, Cell Signaling Technology Cat# 8661,
628 RRID:AB_11217435), rabbit anti-EGFR (1:1000, Cell Signaling Technology Cat# 4267,
629 RRID:AB_2246311), rabbit anti-GAPDH (1:1000, Cell Signaling Technology Cat# 5174,
630 RRID:AB_10622025), mouse anti-Vinculin (1:1000, Thermo Fisher Scientific Cat# 14-9777-80,
631 RRID:AB_2573027), rabbit anti-Merlin (1:1000, Cell Signaling Technology Cat# 12888,
632 RRID:AB_2650551) (see also Table S2).

633 After 2x washes in TBST, membranes were incubated with anti-rabbit or anti-mouse
634 HRP-conjugated secondary antibodies (1:5000, CST#7074, RRID: AB_2099233 or CST#7076,
635 RRID: AB_330924) or fluorophore-conjugated secondary antibodies (1:10,000, LI-COR
636 Biosciences, IRDye 680 LT CAT#925-68020, or IRDye 800CW, CAT#925-32210) in 5%
637 BSA/TBST for 1h at RT. Membranes treated with enhanced chemiluminescence substrate
638 (Thermo Fisher Cat#PI34080) were detected by film (Thomas Sci. Cat#EK-5130) or Licor
639 Odyssey Fc. Membranes treated with fluorophore-conjugated secondary antibodies were
640 imaged on a Licor Odyssey Fc. Normalized protein level changes were calculated using FIJI [83]
641 by measuring the integrated intensity of a set box size encompassing the protein band. The
642 background signal was measured by applying the same box to an adjacent region of the blot
643 and subtracted from the median protein intensity. An equivalent box size was used for
644 reference/loading control protein bands as the protein of interest.
645
646 **Immunofluorescence**
647 Cells were plated on bovine fibronectin-coated (1:75 in PBS, Sigma-Aldrich F1141,
648 CAT#F1141) or collagen-coated (1:100 in PBS, Advanced Biomatrix Cat#5005-B), 96-well,
649 glass-bottom plates (Cellvis CAT# P96-1.5h-N). Cells were fixed in 4% PFA (in PBS, Fisher
650 Scientific Cat#AA433689) for 15 min at room temperature (RT), washed 3x with PBS,
651 permeabilized in 0.2% Triton X-100 for 15 min, and blocked in blocking solution (10% FBS, 5%
652 BSA, 0.1% Triton X-100, 0.01% NaN3 in PBS) for 1h at RT. For conditions with EdU
653 incorporation (10 μM in basal medium, 12-15 min at 37C, Cayman Chemical Cat#20518) prior
654 to fixation, cells were washed 1x with PBS after the blocking step and treated with a click
655 chemistry solution (2 mM CuSO4, 20 mg/mL sodium ascorbate, 3 μM AFDye picolyl azide (488,
656 568, or 647, Click Chemistry Tools Cat# 1276, 1292, or 1300 respectively) in TBS (50 mM Tris,
657 150 mM NaCl, pH 8.3) for 25 min. Following a 1x PBS wash, cells were incubated with primary
658 antibody for 3h at room temperature or overnight at 4C (see also Table S2) in blocking solution,
659 then washed 3x in PBS. Fluorophore-conjugated secondary antibodies (Thermo Fisher
660 Scientific, goat anti-mouse, goat anti-rabbit, 1:1000 in blocking solution) and Hoechst 333342
661 (Thermo Fisher Scientific Cat#H3570, 1:10,000) were incubated on cells for 1h at RT, then
662 washed 3x in PBS. Wells were imaged in 1x PBS or 1x N-acetylcysteine (NAC, 700 mM in
663 ddH2O, pH 7.4, Sigma-Aldrich A7250) imaging buffer for iterative immunofluorescence
664 protocol[33] (4i).
665 For the 4i protocol, wells were then washed 1x in dH2O, treated with elution buffer (0.5M
666 L-glycine (Sigma-Aldrich Cat#G2879), 3M urea (Sigma-Aldrich Cat#U5378), 3M guanidine

667 hydrochloride (Sigma-Aldrich Cat# G3272), 70 mM TCEP-HCl (Goldbio Cat# TCEP50) in
668 ddH2O, pH 2.5) for 20 min on an orbital shaker. After 1x PBS wash, elution was confirmed by
669 fluorescence microscopy. Cells were then blocked with 4i blocking solution (1% BSA + 150 mM
670 maleimide (Sigma-Aldrich Cat# 129585) in PBS) for 30 min, then incubated with the second
671 round of primaries (in blocking solution) for at least 3h RT or overnight at 4C. Secondary
672 staining, imaging in NAC, and subsequent elution and 4i blocking steps were repeated up to 5
673 times. Control wells with secondary antibody treatment alone were used to confirm proper
674 elution of previous antibody rounds. Antibody list and dilutions used for immunofluorescence are
675 listed below and in Table S2:
676
677 **Immunofluorescence Antibodies**
678 The following primary antibodies were used exclusively for round 1 of immunofluorescence
679 staining: rabbit anti-CDK6 (1:1000, Abcam Cat#ab124821, RRID: AB_10999714), rabbit anti-
680 YAP (1:400, Cell Signaling Technology Cat# 14074, RRID:AB_2650491), mouse anti-p27
681 (1:1000, Cell Signaling Technology Cat#3698, RRID:AB_2077832), mouse anti-p21 (1:500, BD
682 Bioscience Cat#556430, RRID:AB_396414), rabbit phospho-AKT(S473)(1:400, Cell Signaling
683 Technology Cat#4060, RRID:AB_2315049), rabbit phospho-MAPK1/2(Thr202/Tyr204)(1:400,
684 Cell Signaling Technology Cat#4370, RRID:AB_2315112), mouse phospho-S6(235/236)(1:800,
685 Cell Signaling Technology Cat#62016, RRID:AB_2799618).
686 The following primary antibodies were used for any round of immunofluorescence:
687 mouse anti-cyclin D1 (1:200, Santa Cruz Biotech Cat#sc-8396, RRID:AB_627344), mouse anti-
688 FRA1 (1:200, Santa Cruz Biotech Cat#sc-28310, RRID: AB_ AB_627632), rabbit anti-Myc
689 (1:800, Cell Signaling Technology Cat#5605, RRID:AB_1903938), mouse anti-Myc tag (1:8,000,
690 Cell Signaling Technology Cat#2276, RRID:AB_331783), mouse anti-N-cadherin (1:200, Santa
691 Cruz Biotech Cat#sc-393933, RRID: AB_2832921), rabbit anti-p27 (1:1600, Cell Signaling
692 Technology Cat#3686, RRID:AB_2077850), rabbit anti-p21 (1:2500, Cell Signaling Technology
693 Cat#2947, RRID:AB_823586), rabbit anti-phospho-Rb(Ser807/811)(1:2500, Cell Signaling
694 Technology Cat#8516, RRID:AB_1117658), rabbit anti-phospho-S6(240/244)(1:2500, Cell
695 Signaling Technology Cat#5364, RRID:AB_10694233), rabbit anti-Skp2 (1:800, Cell Signaling
696 Technology Cat#2652, RRID:AB_11178941), mouse anti-YAP (1:200, Santa Cruz Biotech.
697 Cat#sc-101199,RRID: AB_1131430). Antibodies were previously validated in RPE1[22] and for
698 4i[84], and in this study by drug treatment (including AKT, mTORC1/2, MEK, and LATS1/2
699 inhibitors).

700 The following secondaries were used in variable combination (488, 514 or 568, and
701 647), at 1:1000: goat anti-mouse IgG Alexa Fluor 488 (Thermo Fisher Scientific Cat#A11029,
702 RRID:AB_2534088), goat anti-mouse IgG Alexa Fluor 514 (Thermo Fisher Scientific
703 Cat#A31558, RRID:AB_1037789), goat anti-mouse IgG Alexa Fluor 568 (Thermo Fisher
704 Scientific Cat#A-11031 RRID:AB_144696), goat anti-rabbit IgG Alexa Fluor 568 (Thermo Fisher
705 Scientific Cat#A11036, RRID:AB_1056366), goat anti-rabbit IgG Alexa Fluor 647 (Thermo
706 Fisher Scientific Cat#A21245, RRID:AB_23813).
707
708 **Microscopy**
709 For automated epifluorescence microscopy, cells were imaged on a Ti2-E inverted microscope
710 (Nikon) using penta-band (DAPI/CFP/YFP/TRITC/Cy5, Chroma: 89405) Sedat filter sets with an
711 LED light source (Lumencor Spectra X or Spectra III), Hamamatsu ORCA-fusionBT or ORCA-
712 Flash4.0 V3 sCMOS camera, and 20x objective (Nikon CFI Plan Apo Lambda, 0.75 NA) in a
713 humidified chamber at 37C. 25-30 tiled images were acquired per well in 16-bit mode with 2x2
714 binning. Fixed cells were imaged in 1x N-acetylcysteine imaging buffer. Fluorophores for
715 secondary antibodies were previously optimized to minimize bleed-through[81].
716
717 **RNA sequencing experimental conditions**
718 WT and doxycycline-inducible YAP5SA cells were seeded at 38,000 cells per well of 96-well,
719 optical-grade plates (Sigma-Aldrich Cat#CLS3904) in 1.0% FBS. After ~2h to allow time for
720 adherence to the tissue culture surface, cells were washed with 0.1% FBS then pre-arrested
721 with CDK4/6 inhibitor (palbociclib, 1 uM, SelleckChem CAT#S1116) in either 1.0% FBS or 0.1%
722 FBS for 28-36h prior to doxycycline (500 ng/mL, Sigma-Aldrich CAT#D9891) induction or
723 DMSO control treatment for 6, 12, 24, or 36h in the presence of CDK4/6 inhibitor to maintain
724 cells in G0 and prevent additional transcriptional variation due to cell cycle progression. Each
725 experiment (repeated on three separate occasions) was performed in technical duplicate (with 6
726 replicate wells per technical duplicate), reserving one replicate for immunofluorescence staining
727 to confirm quality of cell cycle arrest (by DNA content and EdU incorporation) and the other for
728 harvesting RNA.
729
730 **RNA-seq and analysis**
731 Prior to harvesting, 96-well plates were washed with PBS, aspirated fully and transferred
732 immediately to -80C. RNA was later harvested from the plates by briefly thawing prior to using
733 extraction by RNeasy Mini kit (Qiagen Cat# 74106) and QIAshredder (Qiagen Cat#79654), with

734 pooling of 6 technical replicate wells/condition directly following the lysis step prior to following
735 the manufacturer protocol, including the optional DNase treatment (Qiagen Cat# 79254).
736 Samples were eluted in ultraPure ddH2O and assessed for quality using an Agilent Bioanalyzer
737 TapeStation. Illumina Stranded mRNA library preparation with polyA capture and sequencing
738 was performed on a NovaSeq6000 system (paired-end, 2 x 50) at the Weill Cornell Genome
739 Resources Core Facility over two rounds to get sufficient read depth.
740 Raw reads were checked for quality using FASTQC then aligned to the human genome
741 assembly (GRCh38) with HISAT2 [85] and assigned to genomic features with featureCounts[86].
742 Differential expression analysis was conducted with DESeq2 [87].
743
744 **Image quantifications and analysis**
745 Illumination bias correction, nuclear segmentation, image cropping and alignment across
746 iterative rounds of immunofluorescence, and analysis were performed with a custom MATLAB
747 pipeline (previously published[81] and deposited on Github: https://github.com/MeyerLab/image-
748 analysis-ratnayeke-2021) incorporating local density measurements[22]. For illumination bias
749 correction, images of background autofluorescence from immunofluorescence blocking solution
750 in cell-free wells were taken for each experiment and used to flatten raw images. Cell nuclei
751 were automatically segmented using Hoechst staining, a Gaussian filter, and a curvature-based
752 object splitting algorithm. A segmentation mask from the first round of imaging was used to align
753 subsequent imaging rounds and crop the images for the overlapping regions. Image jitter
754 between 4i rounds was typically less than 500 nm.
755 For nuclear-localized protein stains (EdU, cyclin D1, p27, phospho-Rb, c-Myc, Fra1,
756 SKP2, CDK6, p21), global background subtraction was performed automatically by expanding a
757 7.8 μm ring from the nuclear mask and subtracting the 25th percentile of pixel signal as
758 estimated background. For protein stains with cytoplasmic and nuclear localization (YAP,
759 phospho-S6, phospho-AKT, phospho-ERK, N-cadherin), median background signal was
760 estimated during analysis by manual averaging of background pixels of representative cell-free
761 regions and subtracting as a flat threshold. For quantification of immunofluorescence signals,
762 DNA content was calculated as the total nuclear Hoechst intensity (median intensity x nuclear
763 area); nuclear fluorescence signals were calculated as the median nuclear intensity;
764 cytoplasmic fluorescence signals were calculated as the median cytoplasmic intensity
765 (expanding the nuclear mask with a ring of inner radius 0.65 um and outer radius 3.23 um to
766 minimize the chance of sampling cytoplasm of neighboring cells). To compare experimental

767 replicates, fold-change in immunofluorescence staining was used to account for the variation in
768 staining and real fluorescence unit values.
769 Cell gating for G1-phase cells was performed by distinguishing G0/G1 and G2 cell
770 populations by 2N or 4N DNA context, then selecting cells below the EdU-incorporation
771 threshold (see sample EdU histograms, Figure S1B) with 2N DNA. Otherwise, for calculating
772 percent EdU-positive or percent Rb phosphorylated (all-cell gating), cells across cell cycle
773 phases were analyzed together. Rb phosphorylation was defined by histogram analysis of the
774 bifurcated phospho-Rb stain and calculating the fraction of cells above the threshold cutoff (see
775 sample p-Rb histograms, Figure S1B).
776
777 **Local cell density analysis**
778 Local cell density analysis was adapted from Fan et al., 2021. Briefly, local density was
779 measured by dividing imaging sites (25-30 tiled images/well) into a 3D histogram based on the
780 centroid coordinates of segmented nuclei (10 x 10 grid, MATLAB hist3). The xy location
781 coordinates of each cell centroid were rounded and the number of cells per block was
782 automatically counted, then scaled back to match the original image size (giving numerical
783 output rather than integer values)[22]. The local cell density value assigned for each cell was
784 based on the scaled number of cells in its assigned local density block.
785
786 **Quantification corrections**
787 While cells were counted prior to seeding, final cell plating density varied across experiments,
788 and absolute proliferation levels varied per independent experiment. We therefore assessed
789 both absolute (% EdU, % p-Rb) and fold-change proliferation metrics for assessing drug and
790 condition effect sizes.
791 During the iterative steps of multiplexed immunofluorescence, some cells washed off
792 during later rounds of imaging. As a proxy for null cells, cells that were segmented from the first
793 round of imaging were gated out of the final analysis if their Hoechst value was less than 100
794 RFU for a subsequent imaging round.
795
796 **Statistical Analysis**
797 Statistical analyses were performed using Student's one-sample or paired (MATLAB ttest) and
798 two-sample (MATLAB ttest2) t tests. Linear regressions for data binned by local cell density
799 were performed using fitlm (MATLAB). 95% confidence intervals and SEM are plotted as
800 indicated for representative experiments and summary data.

801 **REFERENCES**

802 1. Moya, I.M., and Halder, G. (2019). Hippo-YAP/TAZ signalling in organ regeneration
803 and regenerative medicine. Nat. Rev. Mol. Cell Biol. *20*, 211–226. 10.1038/s41580-018-
804 0086-y.

805 2. Driskill, J.H., and Pan, D. (2023). Control of stem cell renewal and fate by YAP and
806 TAZ. Nat. Rev. Mol. Cell Biol. *24*, 895–911. 10.1038/s41580-023-00644-5.

807 3. Totaro, A., Panciera, T., and Piccolo, S. (2018). YAP/TAZ upstream signals and
808 downstream responses. Nat. Cell Biol. *20*, 888–899. 10.1038/s41556-018-0142-z.

809 4. Fan, F., He, Z., Kong, L.-L., Chen, Q., Yuan, Q., Zhang, S., Ye, J., Liu, H., Sun, X.,
810 Geng, J., et al. (2016). Pharmacological targeting of kinases MST1 and MST2 augments
811 tissue repair and regeneration. Sci. Transl. Med. *8*, 352ra108.
812 10.1126/scitranslmed.aaf2304.

813 5. Kastan, N., Gnedeva, K., Alisch, T., Petelski, A.A., Huggins, D.J., Chiaravalli, J.,
814 Aharanov, A., Shakked, A., Tzahor, E., Nagiel, A., et al. (2021). Small-molecule
815 inhibition of Lats kinases may promote Yap-dependent proliferation in postmitotic
816 mammalian tissues. Nat. Commun. *12*, 3100. 10.1038/s41467-021-23395-3.

817 6. Namoto, K., Baader, C., Orsini, V., Landshammer, A., Breuer, E., Dinh, K.T., Ungricht,
818 R., Pikiolek, M., Laurent, S., Lu, B., et al. (2024). NIBR-LTSi is a selective LATS kinase
819 inhibitor activating YAP signaling and expanding tissue stem cells in vitro and in vivo.
820 Cell Stem Cell *31*, 554-569.e17. 10.1016/j.stem.2024.03.003.

821 7. Meng, Z., Moroishi, T., and Guan, K.-L. (2016). Mechanisms of Hippo pathway
822 regulation. Genes Dev. *30*, 1–17. 10.1101/gad.274027.115.

823 8. Gumbiner, B.M., and Kim, N.-G. (2014). The Hippo-YAP signaling pathway and contact
824 inhibition of growth. J. Cell Sci. *127*, 709–717. 10.1242/jcs.140103.

825 9. Zhang, N., Bai, H., David, K.K., Dong, J., Zheng, Y., Cai, J., Giovannini, M., Liu, P.,
826 Anders, R.A., and Pan, D. (2010). The Merlin/NF2 tumor suppressor functions through
827 the YAP oncoprotein to regulate tissue homeostasis in mammals. Dev. Cell *19*, 27–38.
828 10.1016/j.devcel.2010.06.015.

829 10. Huang, J., Wu, S., Barrera, J., Matthews, K., and Pan, D. (2005). The Hippo signaling
830 pathway coordinately regulates cell proliferation and apoptosis by inactivating Yorkie,
831 the Drosophila Homolog of YAP. Cell *122*, 421–434. 10.1016/j.cell.2005.06.007.

832 11. Benhamouche, S., Curto, M., Saotome, I., Gladden, A.B., Liu, C.-H., Giovannini, M., and
833 McClatchey, A.I. (2010). Nf2/Merlin controls progenitor homeostasis and tumorigenesis
834 in the liver. Genes Dev. *24*, 1718–1730. 10.1101/gad.1938710.

835 12. Yu, F.-X., Zhao, B., and Guan, K.-L. (2015). Hippo pathway in organ size control, tissue
836 homeostasis, and cancer. Cell *163*, 811–828. 10.1016/j.cell.2015.10.044.

837 13. Zhao, B., Ye, X., Yu, J., Li, L., Li, W., Li, S., Yu, J., Lin, J.D., Wang, C.-Y., Chinnaiyan,
838 A.M., et al. (2008). TEAD mediates YAP-dependent gene induction and growth control.
839 Genes Dev. *22*, 1962–1971. 10.1101/gad.1664408.

840 14. Mizuno, T., Murakami, H., Fujii, M., Ishiguro, F., Tanaka, I., Kondo, Y., Akatsuka, S.,
841 Toyokuni, S., Yokoi, K., Osada, H., et al. (2012). YAP induces malignant mesothelioma
842 cell proliferation by upregulating transcription of cell cycle-promoting genes. Oncogene
843 *31*, 5117–5122. 10.1038/onc.2012.5.

844 15. Zanconato, F., Forcato, M., Battilana, G., Azzolin, L., Quaranta, E., Bodega, B., Rosato,
845 A., Bicciato, S., Cordenonsi, M., and Piccolo, S. (2015). Genome-wide association
846 between YAP/TAZ/TEAD and AP-1 at enhancers drives oncogenic growth. Nat. Cell
847 Biol. *17*, 1218–1227. 10.1038/ncb3216.

848 16. Zhang, J., Ji, J.-Y., Yu, M., Overholtzer, M., Smolen, G.A., Wang, R., Brugge, J.S.,
849 Dyson, N.J., and Haber, D.A. (2009). YAP-dependent induction of amphiregulin
850 identifies a non-cell-autonomous component of the Hippo pathway. Nat. Cell Biol. *11*,
851 1444–1450. 10.1038/ncb1993.

852 17. Zhang, H., Pasolli, H.A., and Fuchs, E. (2011). Yes-associated protein (YAP)
853 transcriptional coactivator functions in balancing growth and differentiation in skin. Proc
854 Natl Acad Sci USA *108*, 2270–2275. 10.1073/pnas.1019603108.

855 18. Koo, J.H., Plouffe, S.W., Meng, Z., Lee, D.-H., Yang, D., Lim, D.-S., Wang, C.-Y., and
856 Guan, K.-L. (2020). Induction of AP-1 by YAP/TAZ contributes to cell proliferation and
857 organ growth. Genes Dev. *34*, 72–86. 10.1101/gad.331546.119.

858 19. Liu, X., Li, H., Rajurkar, M., Li, Q., Cotton, J.L., Ou, J., Zhu, L.J., Goel, H.L., Mercurio,
859 A.M., Park, J.-S., et al. (2016). Tead and AP1 coordinate transcription and motility. Cell
860 Rep. *14*, 1169–1180. 10.1016/j.celrep.2015.12.104.

861 20. Lavoie, H., Gagnon, J., and Therrien, M. (2020). ERK signalling: a master regulator of
862 cell behaviour, life and fate. Nat. Rev. Mol. Cell Biol. *21*, 607–632. 10.1038/s41580-020-
863 0255-7.

864 21. Chiasson-MacKenzie, C., and McClatchey, A.I. (2018). Cell-Cell Contact and Receptor
865 Tyrosine Kinase Signaling. Cold Spring Harb. Perspect. Biol. *10*.
866 10.1101/cshperspect.a029215.

867 22. Fan, Y., and Meyer, T. (2021). Molecular control of cell density-mediated exit to
868 quiescence. Cell Rep. *36*, 109436. 10.1016/j.celrep.2021.109436.

869 23. Yang, H.W., Chung, M., Kudo, T., and Meyer, T. (2017). Competing memories of
870 mitogen and p53 signalling control cell-cycle entry. Nature *549*, 404–408.
871 10.1038/nature23880.

872 24. Aoki, K., Kumagai, Y., Sakurai, A., Komatsu, N., Fujita, Y., Shionyu, C., and Matsuda,
873 M. (2013). Stochastic ERK activation induced by noise and cell-to-cell propagation
874 regulates cell density-dependent proliferation. Mol. Cell *52*, 529–540.
875 10.1016/j.molcel.2013.09.015.

876 25. Rubin, S.M., Sage, J., and Skotheim, J.M. (2020). Integrating old and new paradigms of
877 G1/S control. Mol. Cell *80*, 183–192. 10.1016/j.molcel.2020.08.020.

878 26. Zhao, B., Wei, X., Li, W., Udan, R.S., Yang, Q., Kim, J., Xie, J., Ikenoue, T., Yu, J., Li,
879 L., et al. (2007). Inactivation of YAP oncoprotein by the Hippo pathway is involved in
880 cell contact inhibition and tissue growth control. Genes Dev. *21*, 2747–2761.
881 10.1101/gad.1602907.

882 27. Cai, J., Zhang, N., Zheng, Y., de Wilde, R.F., Maitra, A., and Pan, D. (2010). The Hippo
883 signaling pathway restricts the oncogenic potential of an intestinal regeneration program.
884 Genes Dev. *24*, 2383–2388. 10.1101/gad.1978810.

885 28. Lee, M.-J., Byun, M.R., Furutani-Seiki, M., Hong, J.-H., and Jung, H.-S. (2014). YAP
886 and TAZ regulate skin wound healing. J. Invest. Dermatol. *134*, 518–525.
887 10.1038/jid.2013.339.

888 29. Hagenbeek, T.J., Zbieg, J.R., Hafner, M., Mroue, R., Lacap, J.A., Sodir, N.M., Noland,
889 C.L., Afghani, S., Kishore, A., Bhat, K.P., et al. (2023). An allosteric pan-TEAD inhibitor
890 blocks oncogenic YAP/TAZ signaling and overcomes KRAS G12C inhibitor resistance.
891 Nat. Cancer *4*, 812–828. 10.1038/s43018-023-00577-0.

892 30. Kastan, N.R., Oak, S., Liang, R., Baxt, L., Myers, R.W., Ginn, J., Liverton, N., Huggins,
893 D.J., Pichardo, J., Paul, M., et al. (2022). Development of an improved inhibitor of Lats
894 kinases to promote regeneration of mammalian organs. Proc Natl Acad Sci USA *119*,
895 e2206113119. 10.1073/pnas.2206113119.

896 31. Bienvenu, F., Jirawatnotai, S., Elias, J.E., Meyer, C.A., Mizeracka, K., Marson, A.,
897 Frampton, G.M., Cole, M.F., Odom, D.T., Odajima, J., et al. (2010). Transcriptional role
898 of cyclin D1 in development revealed by a genetic-proteomic screen. Nature *463*, 374–
899 378. 10.1038/nature08684.

900 32. Koff, A. (2006). How to decrease p27Kip1 levels during tumor development. Cancer Cell
901 *9*, 75–76. 10.1016/j.ccr.2006.01.020.

902 33. Gut, G., Herrmann, M.D., and Pelkmans, L. (2018). Multiplexed protein maps link
903 subcellular organization to cellular states. Science *361*. 10.1126/science.aar7042.

904 34. Cheng, M., Sexl, V., Sherr, C.J., and Roussel, M.F. (1998). Assembly of cyclin D-
905 dependent kinase and titration of p27Kip1 regulated by mitogen-activated protein kinase
906 kinase (MEK1). Proc Natl Acad Sci USA *95*, 1091–1096. 10.1073/pnas.95.3.1091.

907 35. Polyak, K., Lee, M.H., Erdjument-Bromage, H., Koff, A., Roberts, J.M., Tempst, P., and
908 Massagué, J. (1994). Cloning of p27Kip1, a cyclin-dependent kinase inhibitor and a
909 potential mediator of extracellular antimitogenic signals. Cell *78*, 59–66. 10.1016/0092-
910 8674(94)90572-x.

911 36. Croci, O., De Fazio, S., Biagioni, F., Donato, E., Caganova, M., Curti, L., Doni, M.,
912 Sberna, S., Aldeghi, D., Biancotto, C., et al. (2017). Transcriptional integration of
913 mitogenic and mechanical signals by Myc and YAP. Genes Dev. *31*, 2017–2022.
914 10.1101/gad.301184.117.

915 37. Monroe, T.O., Hill, M.C., Morikawa, Y., Leach, J.P., Heallen, T., Cao, S., Krijger,
916 P.H.L., de Laat, W., Wehrens, X.H.T., Rodney, G.G., et al. (2019). YAP partially
917 reprograms chromatin accessibility to directly induce adult cardiogenesis in vivo. Dev.
918 Cell *48*, 765-779.e7. 10.1016/j.devcel.2019.01.017.

919 38. Cordenonsi, M., Zanconato, F., Azzolin, L., Forcato, M., Rosato, A., Frasson, C., Inui,
920 M., Montagner, M., Parenti, A.R., Poletti, A., et al. (2011). The Hippo transducer TAZ
921 confers cancer stem cell-related traits on breast cancer cells. Cell *147*, 759–772.
922 10.1016/j.cell.2011.09.048.

923 39. Xie, Q., Chen, J., Feng, H., Peng, S., Adams, U., Bai, Y., Huang, L., Li, J., Huang, J.,
924 Meng, S., et al. (2013). YAP/TEAD-mediated transcription controls cellular senescence.
925 Cancer Res. *73*, 3615–3624. 10.1158/0008-5472.CAN-12-3793.

926 40. Zhang, S., Chen, Q., Liu, Q., Li, Y., Sun, X., Hong, L., Ji, S., Liu, C., Geng, J., Zhang,
927 W., et al. (2017). Hippo Signaling Suppresses Cell Ploidy and Tumorigenesis through
928 Skp2. Cancer Cell *31*, 669-684.e7. 10.1016/j.ccell.2017.04.004.

929 41. Kim, M., Kim, T., Johnson, R.L., and Lim, D.-S. (2015). Transcriptional co-repressor
930 function of the hippo pathway transducers YAP and TAZ. Cell Rep. *11*, 270–282.
931 10.1016/j.celrep.2015.03.015.

932 42. Diehl, J.A., Cheng, M., Roussel, M.F., and Sherr, C.J. (1998). Glycogen synthase kinase-
933 3beta regulates cyclin D1 proteolysis and subcellular localization. Genes Dev. *12*, 3499–
934 3511. 10.1101/gad.12.22.3499.

935 43. Nakayama, K., Nagahama, H., Minamishima, Y.A., Miyake, S., Ishida, N., Hatakeyama,
936 S., Kitagawa, M., Iemura, S., Natsume, T., and Nakayama, K.I. (2004). Skp2-mediated
937 degradation of p27 regulates progression into mitosis. Dev. Cell *6*, 661–672.
938 10.1016/s1534-5807(04)00131-5.

939 44. Malek, N.P., Sundberg, H., McGrew, S., Nakayama, K., Kyriakides, T.R., and Roberts,
940 J.M. (2001). A mouse knock-in model exposes sequential proteolytic pathways that
941 regulate p27Kip1 in G1 and S phase. Nature *413*, 323–327. 10.1038/35095083.

942 45. Shao, D.D., Xue, W., Krall, E.B., Bhutkar, A., Piccioni, F., Wang, X., Schinzel, A.C.,
943 Sood, S., Rosenbluh, J., Kim, J.W., et al. (2014). KRAS and YAP1 converge to regulate
944 EMT and tumor survival. Cell *158*, 171–184. 10.1016/j.cell.2014.06.004.

945 46. Wang, X., Freire Valls, A., Schermann, G., Shen, Y., Moya, I.M., Castro, L., Urban, S.,
946 Solecki, G.M., Winkler, F., Riedemann, L., et al. (2017). YAP/TAZ Orchestrate VEGF
947 Signaling during Developmental Angiogenesis. Dev. Cell *42*, 462-478.e7.
948 10.1016/j.devcel.2017.08.002.

949 47. Komuro, A., Nagai, M., Navin, N.E., and Sudol, M. (2003). WW domain-containing
950 protein YAP associates with ErbB-4 and acts as a co-transcriptional activator for the
951 carboxyl-terminal fragment of ErbB-4 that translocates to the nucleus. J. Biol. Chem. *278*,
952 33334–33341. 10.1074/jbc.M305597200.

953 48. He, C., Lv, X., Hua, G., Lele, S.M., Remmenga, S., Dong, J., Davis, J.S., and Wang, C.
954 (2015). YAP forms autocrine loops with the ERBB pathway to regulate ovarian cancer
955 initiation and progression. Oncogene *34*, 6040–6054. 10.1038/onc.2015.52.

956 49. Gregorieff, A., Liu, Y., Inanlou, M.R., Khomchuk, Y., and Wrana, J.L. (2015). Yap-
957 dependent reprogramming of Lgr5(+) stem cells drives intestinal regeneration and cancer.
958 Nature *526*, 715–718. 10.1038/nature15382.

959 50. Yuan, Y., Park, J., Feng, A., Awasthi, P., Wang, Z., Chen, Q., and Iglesias-Bartolome, R.
960 (2020). YAP1/TAZ-TEAD transcriptional networks maintain skin homeostasis by
961 regulating cell proliferation and limiting KLF4 activity. Nat. Commun. *11*, 1472.
962 10.1038/s41467-020-15301-0.

963 51. King, B., Araki, J., Palm, W., and Thompson, C.B. (2020). Yap/Taz promote the
964 scavenging of extracellular nutrients through macropinocytosis. Genes Dev. *34*, 1345–
965 1358. 10.1101/gad.340661.120.

966 52. Gillies, T.E., Pargett, M., Minguet, M., Davies, A.E., and Albeck, J.G. (2017). Linear
967 Integration of ERK Activity Predominates over Persistence Detection in Fra-1
968 Regulation. Cell Syst. *5*, 549-563.e5. 10.1016/j.cels.2017.10.019.

969 53. Edwards, A.C., Stalnecker, C.A., Jean Morales, A., Taylor, K.E., Klomp, J.E., Klomp,
970 J.A., Waters, A.M., Sudhakar, N., Hallin, J., Tang, T.T., et al. (2023). TEAD Inhibition
971 Overcomes YAP1/TAZ-Driven Primary and Acquired Resistance to KRASG12C
972 Inhibitors. Cancer Res. *83*, 4112–4129. 10.1158/0008-5472.CAN-23-2994.

973 54. Vaidyanathan, S., Salmi, T.M., Sathiqu, R.M., McConville, M.J., Cox, A.G., and Brown,
974 K.K. (2022). YAP regulates an SGK1/mTORC1/SREBP-dependent lipogenic program to

975 support proliferation and tissue growth. Dev. Cell *57*, 719-731.e8.
976 10.1016/j.devcel.2022.02.004.

977 55. Tumaneng, K., Schlegelmilch, K., Russell, R.C., Yimlamai, D., Basnet, H., Mahadevan,
978 N., Fitamant, J., Bardeesy, N., Camargo, F.D., and Guan, K.-L. (2012). YAP mediates
979 crosstalk between the Hippo and PI(3)K–TOR pathways by suppressing PTEN via miR-
980 29. Nat. Cell Biol. *14*, 1322–1329. 10.1038/ncb2615.

981 56. Zoncu, R., Efeyan, A., and Sabatini, D.M. (2011). mTOR: from growth signal integration
982 to cancer, diabetes and ageing. Nat. Rev. Mol. Cell Biol. *12*, 21–35. 10.1038/nrm3025.

983 57. Averous, J., Fonseca, B.D., and Proud, C.G. (2008). Regulation of cyclin D1 expression
984 by mTORC1 signaling requires eukaryotic initiation factor 4E-binding protein 1.
985 Oncogene *27*, 1106–1113. 10.1038/sj.onc.1210715.

986 58. Hamaratoglu, F., Willecke, M., Kango-Singh, M., Nolo, R., Hyun, E., Tao, C., Jafar-
987 Nejad, H., and Halder, G. (2006). The tumour-suppressor genes NF2/Merlin and
988 Expanded act through Hippo signalling to regulate cell proliferation and apoptosis. Nat.
989 Cell Biol. *8*, 27–36. 10.1038/ncb1339.

990 59. Striedinger, K., VandenBerg, S.R., Baia, G.S., McDermott, M.W., Gutmann, D.H., and
991 Lal, A. (2008). The neurofibromatosis 2 tumor suppressor gene product, merlin, regulates
992 human meningioma cell growth by signaling through YAP. Neoplasia *10*, 1204–1212.
993 10.1593/neo.08642.

994 60. Yin, F., Yu, J., Zheng, Y., Chen, Q., Zhang, N., and Pan, D. (2013). Spatial organization
995 of Hippo signaling at the plasma membrane mediated by the tumor suppressor
996 Merlin/NF2. Cell *154*, 1342–1355. 10.1016/j.cell.2013.08.025.

997 61. Wada, K.-I., Itoga, K., Okano, T., Yonemura, S., and Sasaki, H. (2011). Hippo pathway
998 regulation by cell morphology and stress fibers. Development *138*, 3907–3914.
999 10.1242/dev.070987.

1000 62. Aragona, M., Panciera, T., Manfrin, A., Giulitti, S., Michielin, F., Elvassore, N., Dupont,
1001 S., and Piccolo, S. (2013). A mechanical checkpoint controls multicellular growth
1002 through YAP/TAZ regulation by actin-processing factors. Cell *154*, 1047–1059.
1003 10.1016/j.cell.2013.07.042.

1004 63. Ong, Y.T., Andrade, J., Armbruster, M., Shi, C., Castro, M., Costa, A.S.H., Sugino, T.,
1005 Eelen, G., Zimmermann, B., Wilhelm, K., et al. (2022). A YAP/TAZ-TEAD signalling
1006 module links endothelial nutrient acquisition to angiogenic growth. Nat. Metab. *4*, 672–
1007 682. 10.1038/s42255-022-00584-y.

1008 64. Su, T., Bondar, T., Zhou, X., Zhang, C., He, H., and Medzhitov, R. (2015). Two-signal
1009 requirement for growth-promoting function of Yap in hepatocytes. eLife *4*.
1010 10.7554/eLife.02948.

1011 65. Chen, Q., Zhang, N., Xie, R., Wang, W., Cai, J., Choi, K.-S., David, K.K., Huang, B.,
1012 Yabuta, N., Nojima, H., et al. (2015). Homeostatic control of Hippo signaling activity
1013 revealed by an endogenous activating mutation in YAP. Genes Dev. *29*, 1285–1297.
1014 10.1101/gad.264234.115.

1015 66. Meyer, K., Lammers, N.C., Bugaj, L.J., Garcia, H.G., and Weiner, O.D. (2023).
1016 Optogenetic control of YAP reveals a dynamic communication code for stem cell fate and
1017 proliferation. Nat. Commun. *14*, 6929. 10.1038/s41467-023-42643-2.

1018 67. Franklin, J.M., Ghosh, R.P., Shi, Q., Reddick, M.P., and Liphardt, J.T. (2020). Concerted
1019 localization-resets precede YAP-dependent transcription. Nat. Commun. *11*, 4581.
1020 10.1038/s41467-020-18368-x.

1021 68. Manning, S.A., Dent, L.G., Kondo, S., Zhao, Z.W., Plachta, N., and Harvey, K.F. (2018).
1022 Dynamic fluctuations in subcellular localization of the hippo pathway effector yorkie
1023 in vivo. Curr. Biol. *28*, 1651-1660.e4. 10.1016/j.cub.2018.04.018.

1024 69. Curto, M., Cole, B.K., Lallemand, D., Liu, C.-H., and McClatchey, A.I. (2007). Contact-
1025 dependent inhibition of EGFR signaling by Nf2/Merlin. J. Cell Biol. *177*, 893–903.
1026 10.1083/jcb.200703010.

1027 70. Moleirinho, S., Hoxha, S., Mandati, V., Curtale, G., Troutman, S., Ehmer, U., and Kissil,
1028 J.L. (2017). Regulation of localization and function of the transcriptional co-activator
1029 YAP by angiomotin. eLife *6*. 10.7554/eLife.23966.

1030 71. Yi, C., Troutman, S., Fera, D., Stemmer-Rachamimov, A., Avila, J.L., Christian, N.,
1031 Persson, N.L., Shimono, A., Speicher, D.W., Marmorstein, R., et al. (2011). A tight
1032 junction-associated Merlin-angiomotin complex mediates Merlin's regulation of
1033 mitogenic signaling and tumor suppressive functions. Cancer Cell *19*, 527–540.
1034 10.1016/j.ccr.2011.02.017.

1035 72. Kapoor, A., Yao, W., Ying, H., Hua, S., Liewen, A., Wang, Q., Zhong, Y., Wu, C.-J.,
1036 Sadanandam, A., Hu, B., et al. (2014). Yap1 activation enables bypass of oncogenic Kras
1037 addiction in pancreatic cancer. Cell *158*, 185–197. 10.1016/j.cell.2014.06.003.

1038 73. Jang, W., Kim, T., Koo, J.S., Kim, S.-K., and Lim, D.-S. (2017). Mechanical cue-induced
1039 YAP instructs Skp2-dependent cell cycle exit and oncogenic signaling. EMBO J. *36*,
1040 2510–2528. 10.15252/embj.201696089.

1041 74. Kossatz, U., Dietrich, N., Zender, L., Buer, J., Manns, M.P., and Malek, N.P. (2004).
1042 Skp2-dependent degradation of p27kip1 is essential for cell cycle progression. Genes
1043 Dev. *18*, 2602–2607. 10.1101/gad.321004.

1044 75. Adachi, Y., Kimura, R., Hirade, K., Yanase, S., Nishioka, Y., Kasuga, N., Yamaguchi,
1045 R., and Ebi, H. (2023). Scribble mis-localization induces adaptive resistance to KRAS

1046 G12C inhibitors through feedback activation of MAPK signaling mediated by YAP-
1047 induced MRAS. Nat. Cancer *4*, 829–843. 10.1038/s43018-023-00575-2.

1048 76. Lin, L., Sabnis, A.J., Chan, E., Olivas, V., Cade, L., Pazarentzos, E., Asthana, S., Neel,
1049 D., Yan, J.J., Lu, X., et al. (2015). The Hippo effector YAP promotes resistance to RAF-
1050 and MEK-targeted cancer therapies. Nat. Genet. *47*, 250–256. 10.1038/ng.3218.

1051 77. Dai, X., Liu, H., Shen, S., Guo, X., Yan, H., Ji, X., Li, L., Huang, J., Feng, X.-H., and
1052 Zhao, B. (2015). YAP activates the Hippo pathway in a negative feedback loop. Cell Res.
1053 *25*, 1175–1178. 10.1038/cr.2015.101.

1054 78. Moroishi, T., Park, H.W., Qin, B., Chen, Q., Meng, Z., Plouffe, S.W., Taniguchi, K., Yu,
1055 F.-X., Karin, M., Pan, D., et al. (2015). A YAP/TAZ-induced feedback mechanism
1056 regulates Hippo pathway homeostasis. Genes Dev. *29*, 1271–1284.
1057 10.1101/gad.262816.115.

1058 79. Nardone, G., Oliver-De La Cruz, J., Vrbsky, J., Martini, C., Pribyl, J., Skládal, P., Pešl,
1059 M., Caluori, G., Pagliari, S., Martino, F., et al. (2017). YAP regulates cell mechanics by
1060 controlling focal adhesion assembly. Nat. Commun. *8*, 15321. 10.1038/ncomms15321.

1061 80. Pastushenko, I., Mauri, F., Song, Y., de Cock, F., Meeusen, B., Swedlund, B., Impens, F.,
1062 Van Haver, D., Opitz, M., Thery, M., et al. (2021). Fat1 deletion promotes hybrid EMT
1063 state, tumour stemness and metastasis. Nature *589*, 448–455. 10.1038/s41586-020-03046-
1064 1.

1065 81. Ratnayeke, N., Baris, Y., Chung, M., Yeeles, J.T.P., and Meyer, T. (2023). CDT1 inhibits
1066 CMG helicase in early S phase to separate origin licensing from DNA synthesis. Mol.
1067 Cell *83*, 26-42.e13. 10.1016/j.molcel.2022.12.004.

1068 82. Ran, F.A., Hsu, P.D., Wright, J., Agarwala, V., Scott, D.A., and Zhang, F. (2013).
1069 Genome engineering using the CRISPR-Cas9 system. Nat. Protoc. *8*, 2281–2308.
1070 10.1038/nprot.2013.143.

1071 83. Schindelin, J., Arganda-Carreras, I., Frise, E., Kaynig, V., Longair, M., Pietzsch, T.,
1072 Preibisch, S., Rueden, C., Saalfeld, S., Schmid, B., et al. (2012). Fiji: an open-source
1073 platform for biological-image analysis. Nat. Methods *9*, 676–682. 10.1038/nmeth.2019.

1074 84. Stallaert, W., Kedziora, K.M., Taylor, C.D., Zikry, T.M., Ranek, J.S., Sobon, H.K.,
1075 Taylor, S.R., Young, C.L., Cook, J.G., and Purvis, J.E. (2022). The structure of the
1076 human cell cycle. Cell Syst. *13*, 230-240.e3. 10.1016/j.cels.2021.10.007.

1077 85. Kim, D., Paggi, J.M., Park, C., Bennett, C., and Salzberg, S.L. (2019). Graph-based
1078 genome alignment and genotyping with HISAT2 and HISAT-genotype. Nat. Biotechnol.
1079 *37*, 907–915. 10.1038/s41587-019-0201-4.

1080 86. Liao, Y., Smyth, G.K., and Shi, W. (2014). featureCounts: an efficient general purpose
1081 program for assigning sequence reads to genomic features. Bioinformatics *30*, 923–930.
1082 10.1093/bioinformatics/btt656.

1083 87. Love, M.I., Huber, W., and Anders, S. (2014). Moderated estimation of fold change and
1084 dispersion for RNA-seq data with DESeq2. Genome Biol. *15*, 550. 10.1186/s13059-014-
1085 0550-8.

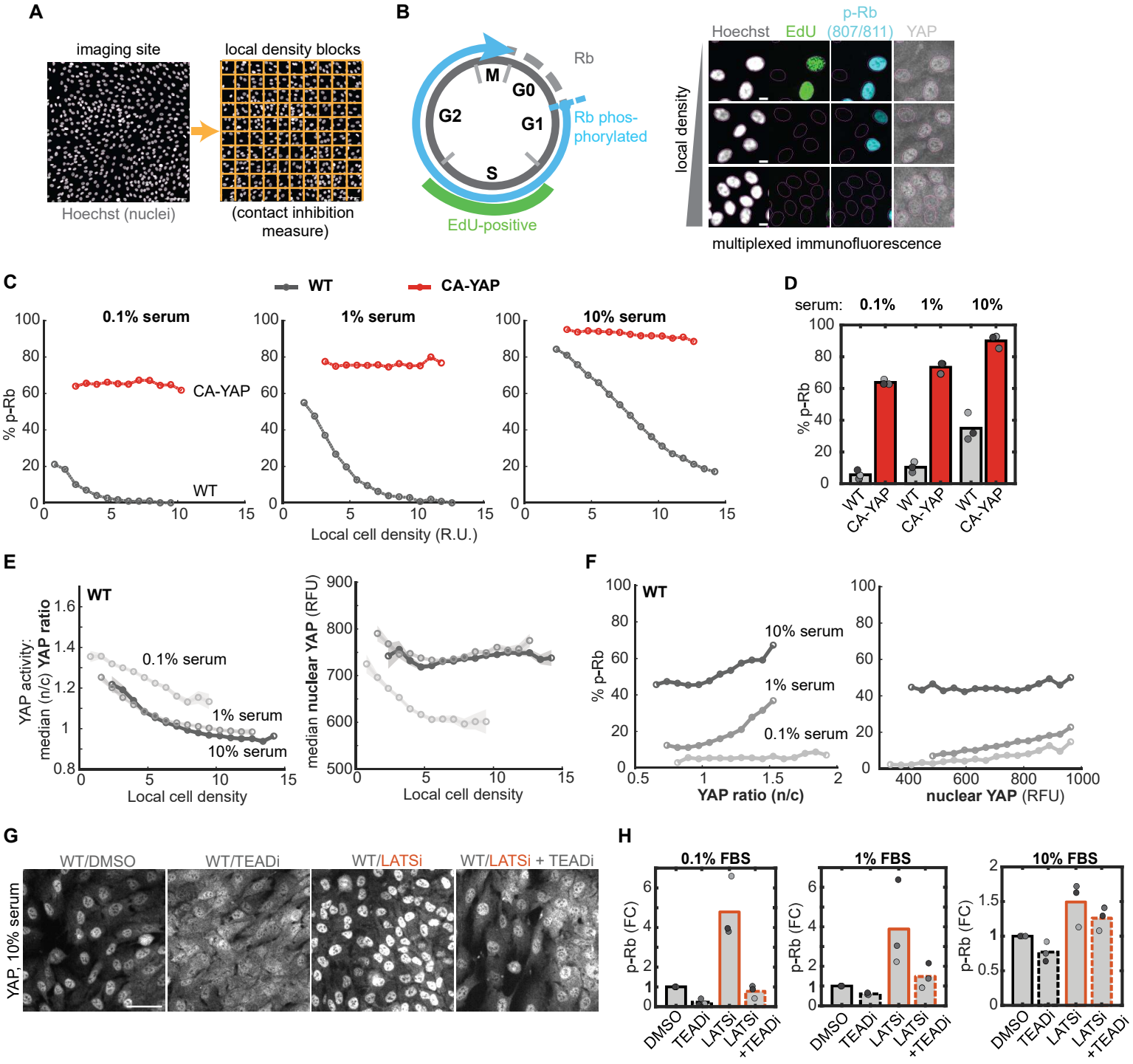

Figure 1. Contact inhibition of YAP opposes mitogen stimulation in a balance mechanism that controls proliferation

1086 **Figure 1. Contact inhibition of YAP opposes mitogen stimulation in a balance mechanism**
1087 **that controls proliferation**
1088
1089 **A)** Local cell density metric by subdividing images into 10 x 10 grids and counting the cells (by
1090 centroid of segmented nucleus) for each block (see also STAR Methods, scale bar = 100 μm).
1091 **B)** Left: Diagram of cell cycle phases: EdU incorporation marks S-phase, Rb
1092 hyperphosphorylation (p-Rb, S807/811) cycling cells. Right: sample images of wildtype (WT)
1093 RPE1 cells at increasing local cell density: Hoechst for DNA (white), EdU for S-phase cells
1094 (green), p-Rb for cycling cells (blue), and YAP (grey). Magenta outline is the automated nuclear
1095 mask (scale bar = 10 μm).
1096 **C)** Local cell density (relative units, R.U.) was measured by binning cell numbers per local block
1097 area. The percent of Rb-phosphorylated cells was calculated per local density bin for WT and
1098 CA-YAP cells maintained in increasing serum levels (0.1%, 1%, or 10%) for 36h, n > 20,000
1099 cells/condition. See also **Figure S1**.
1100 **D)** Mean percent p-Rb for cells treated as in (C). n = 3 independent experiments. Student's t-
1101 test: $p=6.86x10^{-6}$ (0.1% serum), $p=2.50x10^{-5}$ (1% serum), $p = 5.90x10^{-4}$ (10% serum).
1102 **E)** Median nuclear/cytoplasmic (n/c) YAP ratio (left) and nuclear YAP levels (right, real
1103 fluorescent units, R.F.U.) per local density bin for WT cells treated as in (C), n > 20,000
1104 cells/condition. Shaded error bars are 95% confidence intervals.
1105 **F)** Percent p-Rb for WT cells binned by their YAP ratio (left) or nuclear YAP levels (right).
1106 **G**) Representative images of YAP staining for WT cells treated with TEAD inhibitor (TEADi, 0.5
1107 μM GNE-7883), LATS inhibitor (LATSi, 0.5 μM TDI-011536) or in combination in 10% serum for
1108 24h.
1109 **H)** Fold-change in percent p-Rb for WT cells treated with TEADi, LATSi, or in combination,
1110 normalized to DMSO in 0.1% (left), 1% (middle), or 10% serum (right). N = 3 independent
1111 experiments.
1112 All binned plots have n>100 cells/bin and >20,000 cells/condition.

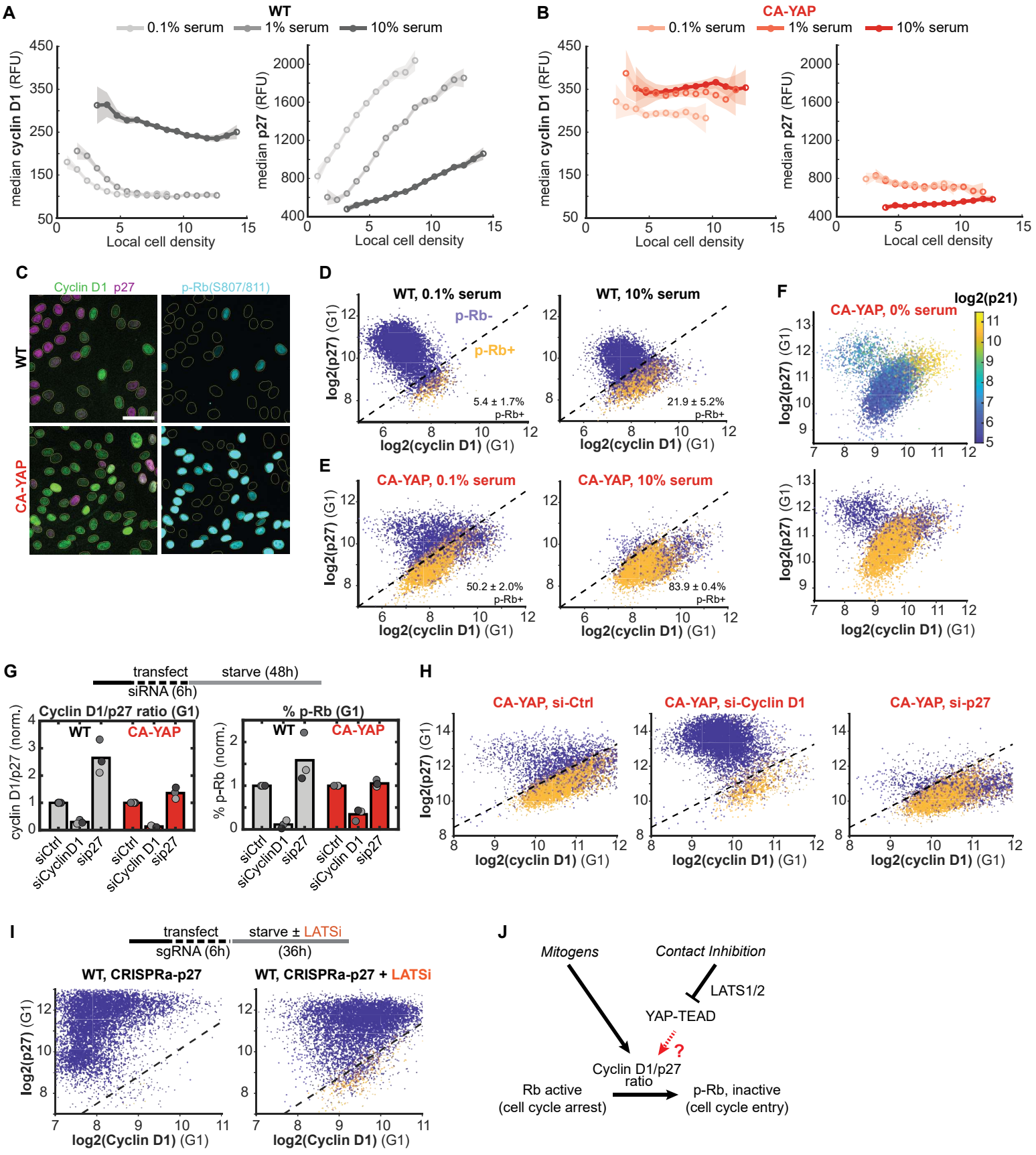

Figure 2. YAP-regulated cell cycle entry and exit is dictated by a cyclin D1/p27 threshold

1113 **Figure 2. YAP-regulated cell cycle entry and exit is dictated by a cyclin D1/p27 threshold**
1114
1115 **A-B)** Median levels (real fluorescent units (RFU)) of cyclin D1 (left) and p27 (right) per local cell
1116 density bin for WT (A) and CA-YAP (B) cells at 0.1%, 1%, and 10% serum. Binned data only
1117 include G1-gated cells, n > 100 cells/bin. Shaded error bars are 95% confidence intervals, n >
1118 15,000 cells per condition. Data are representative of 2 independent experiments.
1119 **C**) Representative images of multiplexed immunofluorescence staining comparing cyclin D1
1120 (green) and p27 levels (magenta) with aligned p-Rb stain (cyan with gray nuclear mask overlay)
1121 in WT or CA-YAP cells. Scale bar = 50 µm.
1122 **D-E**) Single-cell scatterplots of co-stained cyclin D1 and p27 levels (log2-transformed), colored
1123 by p-Rb (purple, p-Rb-negative; orange, p-Rb-positive) in WT (D) and CA-YAP (E). Left, 0.1%
1124 serum; right, 10% serum. Mean ± SD of 2 independent experiments.
1125 **F**) Representative single-cell scatterplot of serum-starved CA-YAP cells co-stained for cyclin D1
1126 and p27 protein levels, colored by p21 protein levels (top: parula color scale) or p-Rb status
1127 (bottom: purple, p-Rb-negative; orange, p-Rb-positive).
1128 **G**) Top: experimental conditions for siRNA transfection followed by 48h serum starvation.
1129 Bottom: mean cyclin D1/p27 ratio (left) and p-Rb (right) for WT and CA-YAP cells transfected
1130 with siRNA against cyclin D1 and p27, normalized to non-targeting control (siCtrl). N = 3
1131 independent experiments.
1132 **H**) Single-cell scatterplots of co-stained cyclin D1 and p27 levels colored by p-Rb for CA-YAP
1133 cells treated as in (G).
1134 **I)** Top: experimental conditions for sgRNA-mediated overexpression (CRISPRa) of p27 in
1135 dCas9-expressing WT cells treated with DMSO or LATSi (0.5 µM TDI-011536). Bottom: Single-
1136 cell scatterplots of co-stained cyclin D1 and p27 levels colored by p-Rb for p27-overexpressing
1137 cells treated with DMSO (left) or LATSi (right).
1138 **J**) Schematic of mitogen signaling and contact inhibition of YAP-TEAD activity converging on
1139 the cyclin D1/p27 ratio to control whether cells enter or exit the cell cycle.
1140 Dashed lines approximate separation of p-Rb-positive and p-Rb-negative cell populations.
1141 Single-cell data are representative of 2 independent experiments, with n = 8,000 random
1142 cells/scatter plot and gated for G1-phase (defined as 2N DNA/EdU-negative status). See also
1143 **Figure S2**.
1144

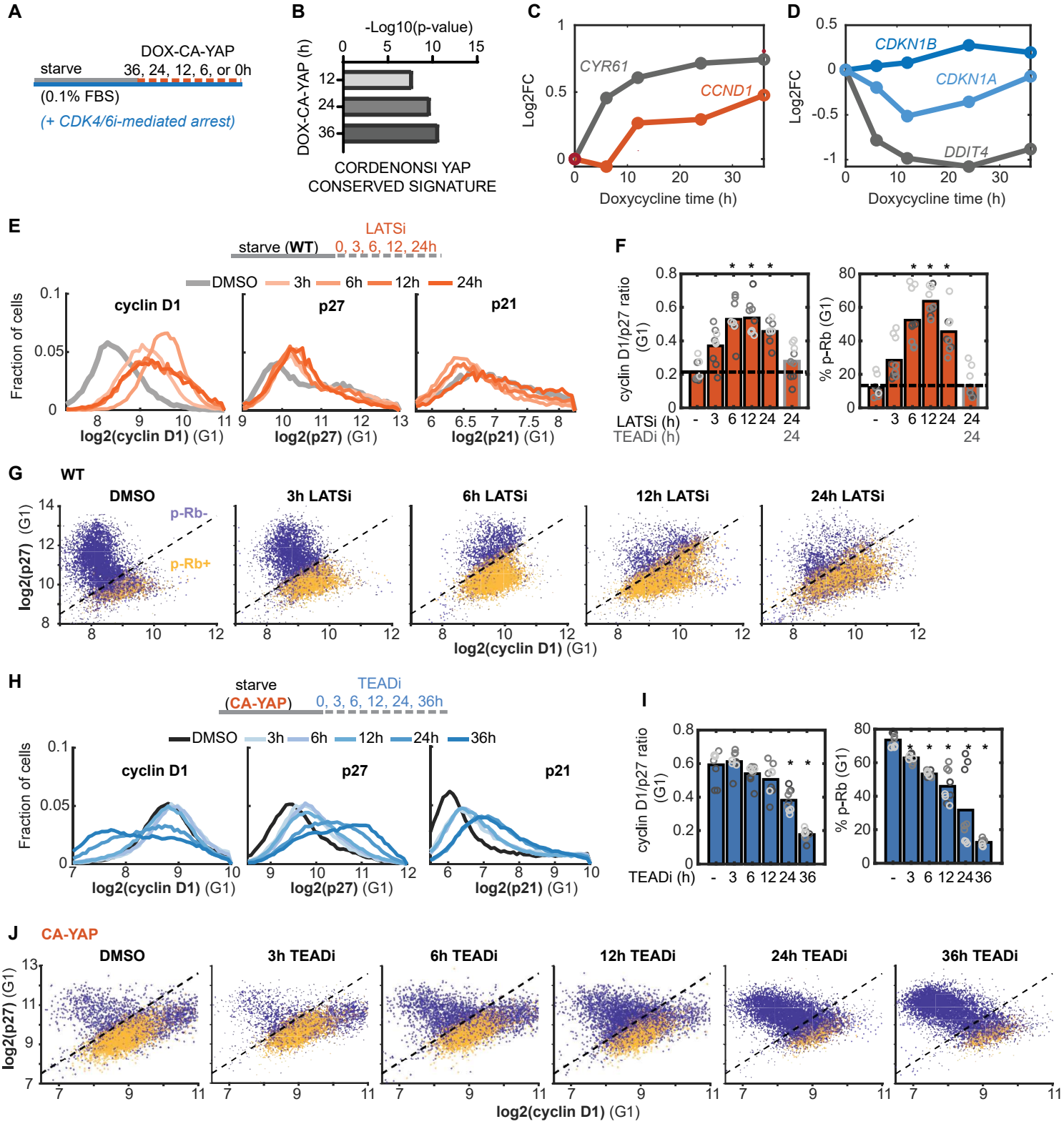

Figure 3. Delayed YAP-mediated control of the nuclear cyclin D1/p27 ratio and cell cycle arrest

1145 **Figure 3. Delayed YAP-mediated control of the cyclin D1/p27 ratio and cell cycle arrest**
1146
1147 **A)** Schematic for CA-YAP expression in RPE1 cells. RNA-sequencing performed in confluent
1148 cells pre-conditioned at 0.1% and palbociclib-arrested (CDK4/6i, 1 μM), prior to doxycycline-
1149 induction over 36h (0.5 μg/mL DOX). See also **Figure S3** and STAR METHODS.
1150 **B)** Up-regulated genes (q<0.05, Log2 fold-change >1) for 12, 24, and 36h YAP induction
1151 showed the Cordenonsi YAP signature (using ToppGene)[38].
1152 **C-D)** Log2 fold-change (Log2FC) induction (C) of *CYR61* (canonical YAP target gene, grey)
1153 compared with *CCND1* (cyclin D1, red) and (D) regulation of DDIT4 (suppressed YAP target
1154 gene, grey), *CDKN1A* (p21, dark blue), and *CDKN1B* (p27, blue) at times since
1155 overexpression. Adjusted p-values (NS at all other time points): *CCND1*, 3.17×10^{-4} (12h), 4.45
1156 $\times 10^{-5}$ (24h), 3.96×10^{-12} (36h); *CDKN1A*, 8.65×10^{-7} (12h), 9.5×10^{-4} (24h); *CDKN1B*, 0.0012 (24h),
1157 0.0312 (36h).
1158 **E)** Top: Experimental conditions for LATSi treatment (0.5 μM TDI-011536) of serum-starved WT
1159 cells for 0-24h. Bottom: Histogram distribution of cyclin D1, p27, and p21 protein levels over
1160 LATSi time course.
1161 **F)** Mean cyclin D1/p27 ratio (left) and percent p-Rb (right) for cells treated as in (E). n = 3
1162 independent experiments and 3 well-replicates/experiment, as indicated by matched
1163 colors. Student's t-test: cyclin D1/p27, p = 0.0062 (6h), 0.0022 (12h), 2.63×10^{-4} (24h); p-Rb, p =
1164 0.0217 (6h), 4.12×10^{-4} (12h), 0.0087 (24h).
1165 **G)** Single-cell scatterplots of cyclin D1 and p27 protein levels colored by p-Rb status (purple, p-
1166 Rb-negative; orange, p-Rb-positive).
1167 **H)** Top: experimental conditions for TEADi treatment (1 μM GNE-7883) of serum-starved CA-
1168 YAP cells. Bottom: Histogram distribution of log2-transformed cyclin D1, p27, and p21 protein
1169 levels over TEADi time course.
1170 **I)** Mean cyclin D1/p27 ratio (left) and percent p-Rb (right) for cells treated as in (H). n = 3
1171 biological replicates, where well-replicates are indicated by matched colors. Student's t-test:
1172 cyclin D1/p27 ratio, p = 0.027 (24h), p = 0.0015 (36h); % p-Rb, p = 0.0188 (3h), p = 0.0011 (6h),
1173 0.0119 (12h), p = 0.0481 (24h), $p = 1.98 \times 10^{-5}$ (36h).
1174 **J)** Single-cell scatterplots of log2-transformed cyclin D1 and p27 protein levels colored by p-Rb
1175 status for cells treated as in (H).
1176 All histogram and single-cell data (n = 8,000 cells/scatterplot) are representative of 3
1177 independent experiments.
1178

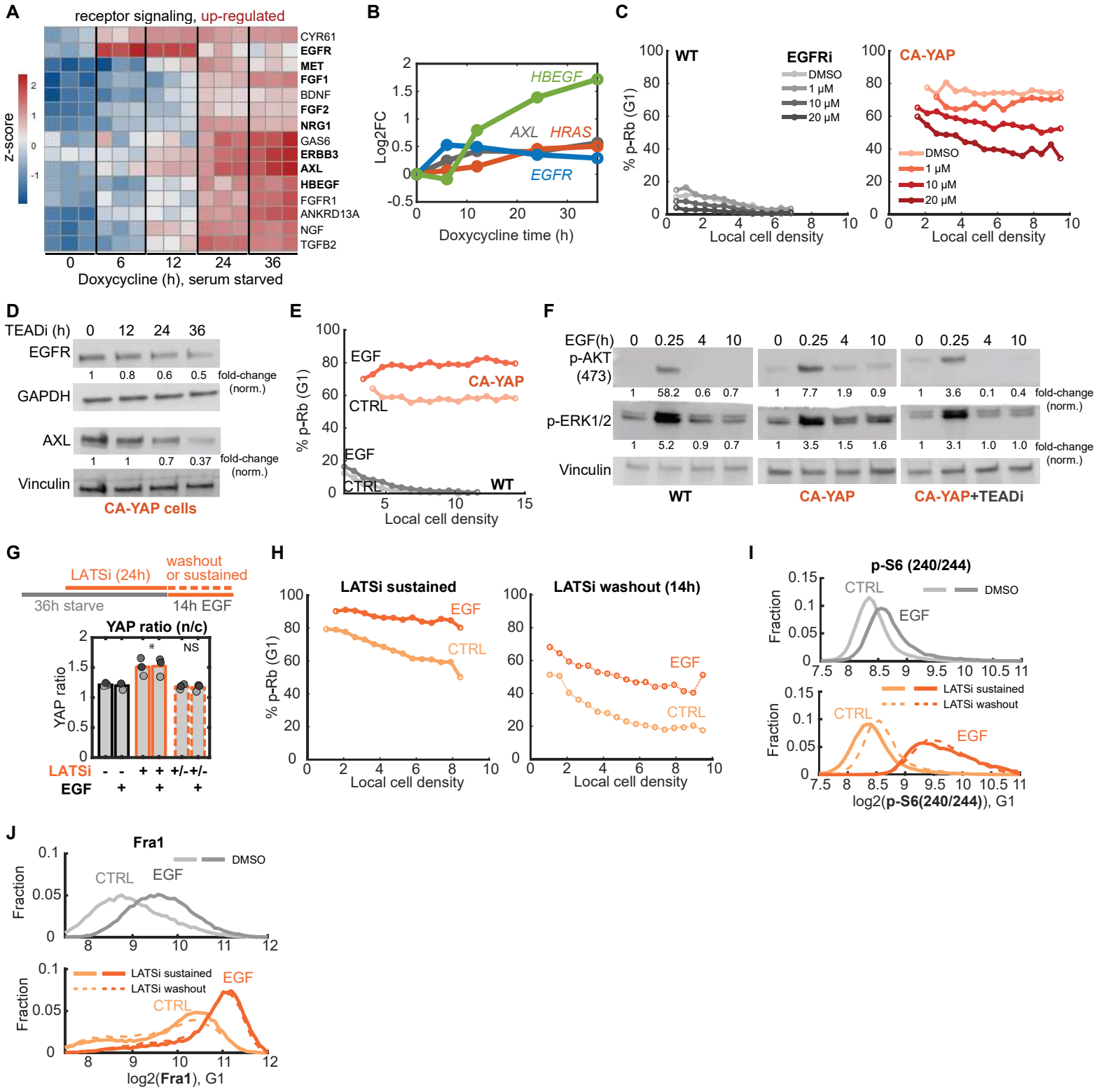

Figure 4. YAP activation induces proliferation by increasing EGFR signaling

1179 **Figure 4. YAP activation induces proliferation by increasing EGFR signaling**
1180
1181 **A)** Heatmap representation of differential expression (row z-score) of select up-regulated ligand
1182 and receptor genes, grouped by 3 independent replicates and time points.
1183 **B)** Log2 fold-change (Log2FC) of select receptor signaling-related genes, *AXL* (direct YAP
1184 target grey), *EGFR* (blue), *HBEGF* (green), and *HRAS* (red). Adjusted p-values: *AXL,* 6.20×10^{-4}
1185 (6h), 9.11×10^{-12} (12h), 2.33×10^{-11}(24h), 2.19×10^{-21} (36h); *EGFR,* 4.97×10^{-16} (6h), 1.07×10^{-14}
1186 (12h), 1.07×10^{-8} (24h), 1.23×10^{-5} (36h); *HBEGF*, 3.90×10^{-4} (12h), 8.57×10^{-12} (24h), 5.24×10^{-18}
1187 (36h); *HRAS*, 4.10×10^{-4} (24h), 6.05×10^{-5} (36h).
1188 **C)** Percent p-Rb binned by local cell density for WT (left) and CA-YAP (right) cells serum-
1189 starved and treated with gefitinib (EGFRi, 0-20 μM) for 24h. See also **Figure S4.**
1190 **D)** Western blot analysis of EGFR and AXL from whole-cell lysates of serum-starved CA-YAP
1191 cells treated with TEADi for 0-36h, with GAPDH and Vinculin loading controls. Values indicate
1192 fold-change difference relative to 0h control (after normalization to loading control). Data are
1193 representative of 2 independent experiments.
1194 **E)** Percent p-Rb binned by local density for serum-starved WT and CA-YAP cells after 14h (25
1195 ng/mL). Data are representative of 2 independent experiments, n > 25,000 cells/condition.
1196 **F)** Western blot analysis of AKT and ERK phosphorylation levels in whole-cell lysates of serum-
1197 starved WT (left), CA-YAP (middle), and TEADi pre-treated CA-YAP cells (right) after 0-10h
1198 EGF treatment (25 ng/mL). Values normalized to loading control and fold-change relative to 0h
1199 control.
1200 **G)** Top: experimental conditions for serum-starvation of WT cells, pre-treatment with LATSi, and
1201 sustained or washout of LATSi during 14h EGF treatment (25 ng/mL). Bottom: Mean YAP ratio
1202 (n/c) for treatment conditions. N = 3 independent experiments, matched colors indicate
1203 conditions from the same experimental replicate. Student's t-test, YAP ratio: LATSi sustained,
1204 p= 0.0278 (CTRL), 0.027 (EGF); LATSi washout, not significant (NS).
1205 **H)** Percent p-Rb binned by local cell density for cells with LATSi sustained (left) or washout
1206 (right) with or without EGF treatment (n > 20,000 cells/condition).
1207 **I-J)** Histogram distribution of phosphorylated-S6 (p-S6 240/244, I) and Fra1 protein distributions
1208 for DMSO-treated (top) or LATSi-pretreated cells (bottom, LATSi sustained and washout). Data
1209 are representative of 3 independent experiments.
1210 All single-cell data represent values from G1-gated cells.
1211

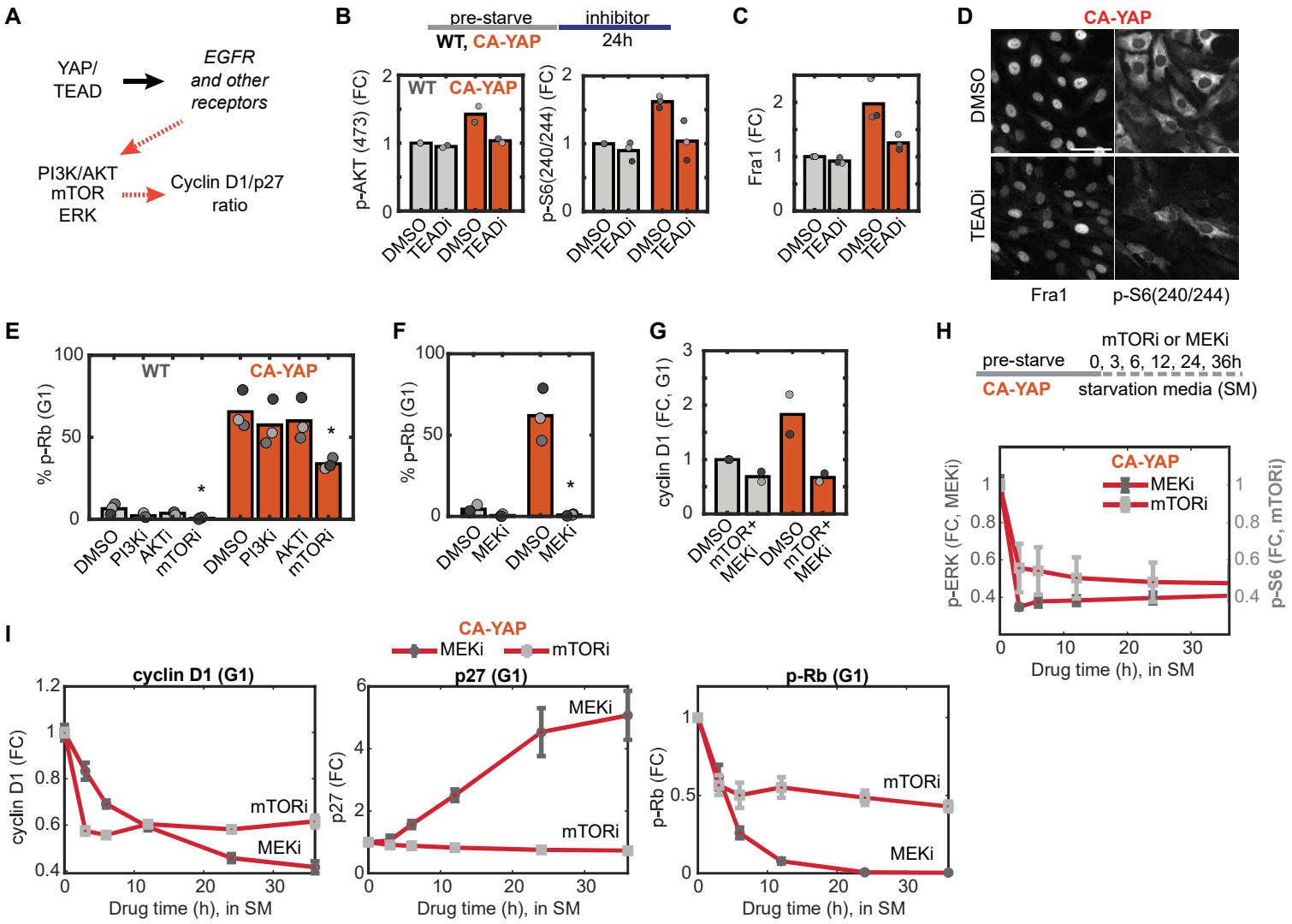

Figure 5. YAP activation signals through ERK and mTOR to increase the cyclin D1/p27 ratio

1212 **Figure 5. YAP activation signals through ERK and mTOR to increase the cyclin D1/p27**
1213 **ratio**
1214
1215 **A)** Schematic representation of proposed indirect regulation of cyclin D1/p27 ratio by
1216 YAP/TEAD via EGFR-activated signaling pathways.
1217 **B-C)** Top: experimental conditions for serum-starvation of WT and CA-YAP cells followed by
1218 24h treatment with TEAD inhibitor for 24h in starvation media. Bottom: Mean fold-change (FC)
1219 in protein levels of p-AKT(473, left) and p-S6(240/244, right) (B) and Fra1 (C) for serum-starved
1220 WT and CA-YAP cells treated with TEADi for 24h (normalized to WT/DMSO condition). N = 2
1221 (p-AKT) or 3 (p-S6, Fra1) independent experiments.
1222 **D)** Representative multiplexed images for Fra1 and p-S6(240/244) staining in CA-YAP cells
1223 treated with TEADi as in (B). Scale bar = 50 μm.
1224 **E-F)** Mean percentage p-Rb for WT and CA-YAP cells treated with PI3K (LY294002, 10 μM),
1225 AKT (MK2206, 200 nM), or mTORC1/2 (Torin2, 100 nM) inhibitors (E) or MEK (PD0325901,
1226 100 nM) inhibitor (F) as in (B). N = 3 independent experiments. Student's t-test: WT/mTORi, p =
1227 0.0372; CA-YAP/mTORi, p = 0.0103 (E). CA-YAP/MEKi, p = 0.0028 (F). See also **Figure S5**.
1228 **G)** Mean FC in cyclin D1 protein levels for WT and CA-YAP cells treated with combined mTORi
1229 and MEKi relative to WT/DMSO condition as in (B). N = 2 independent experiments.
1230 **H)** Top: experiment conditions for mTORi or MEKi time course treatment of serum-starved CA-
1231 YAP cells. Bottom: fold-change in p-ERK (MEKi-treated, dark grey) and p-S6(240/244, mTORi-
1232 treated, light grey) following drug treatment; mean ± SEM (n = 2 independent experiments, 2-3
1233 replicate wells/experiment).
1234 **I)** Fold-change in protein levels of cyclin D1, p27, and p-Rb for MEKi and mTORi for CA-YAP
1235 cells treated as in (H). Mean ± SEM.
1236

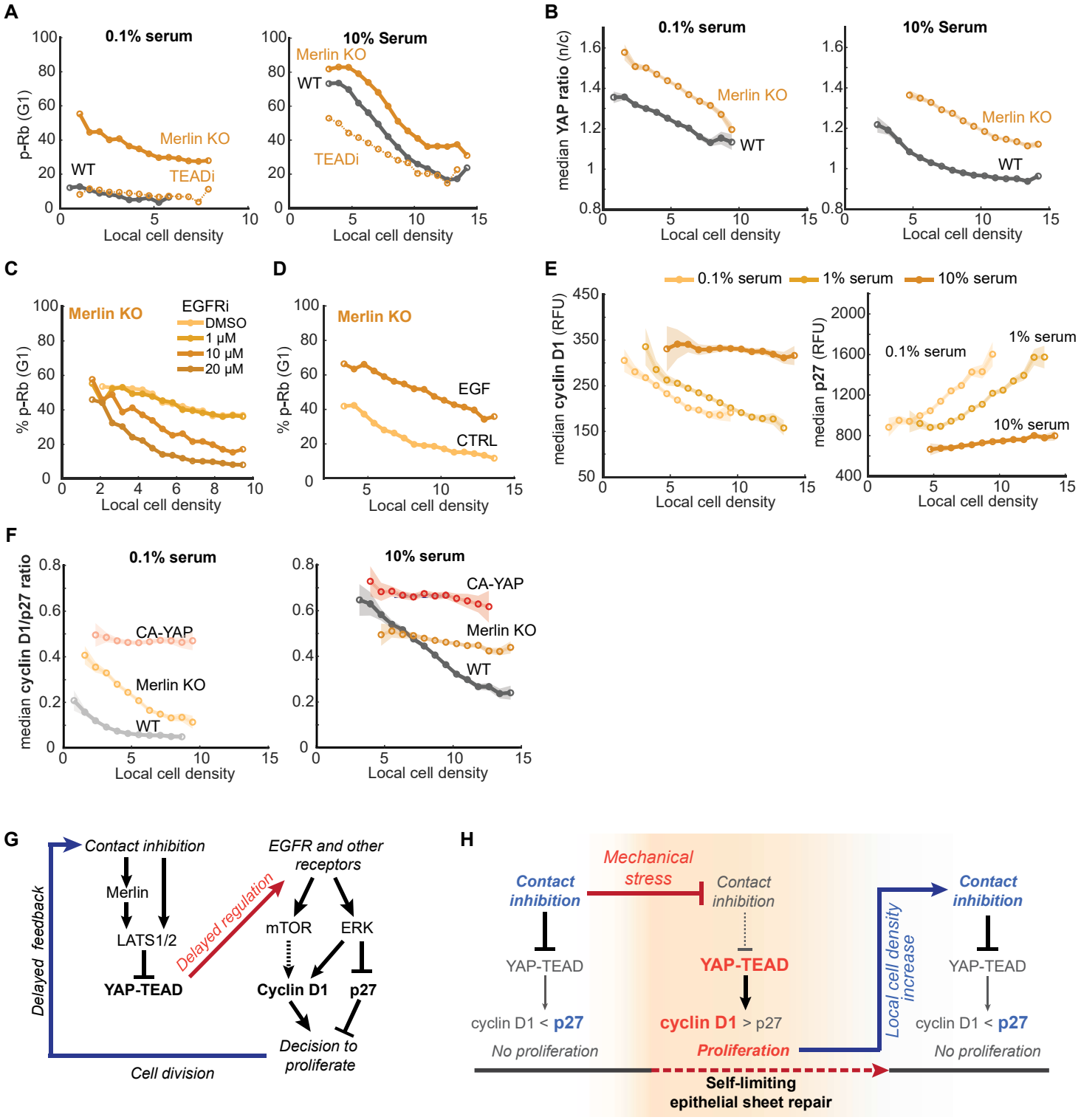

Figure 6. Partial activation of YAP by Merlin knockout can be reversed by increased contact inhibition

1237 **Figure 6. Partial activation of YAP by Merlin knockout can be reversed by increased**
1238 **contact inhibition**
1239
1240 **A)** TEAD-dependent hyperproliferation of Merlin KO cells. Percent p-Rb binned by local density
1241 for Merlin knockout cells (Merlin KO, yellow) in 0.1% (left) or 10% serum (right) treated with
1242 DMSO or TEADi (0.5 M) compared with WT cells (grey).
1243 **B)** Median YAP ratio (n/c) binned by local cell density for Merlin KO cells in 0.1% or 10% serum,
1244 compared with WT cells (same experiment as in **Figure 1E**). Data are representative of 3
1245 independent experiments. Shaded error are 95% confidence intervals.
1246 **C)** Percent p-Rb binned by local density for serum-starved Merlin KO cells treated with gefitinib
1247 (EGFRi) as in Figure 4C. Data are representative of 2 independent experiments.
1248 **D)** Percent p-Rb binned by local cell density for serum-starved Merlin KO cells with control
1249 (CTRL) or EGF (25 ng/mL) treatment for 12h. Data are representative of 2 independent
1250 experiments.
1251 **E)** Median cyclin D1 (left) or p27 (right) protein levels for Merlin KO cells in titrated serum.
1252 Shaded error are 95% confidence intervals. Data are representative of 2 independent
1253 experiments.
1254 **F)** Median cyclin D1/p27 ratio binned by local cell density for WT (grey), Merlin KO (yellow), and
1255 CA-YAP cells (red) in 0.1% (left) or 10% serum (right). Shaded error are 95% confidence
1256 intervals.
1257 **G)** Model for Hippo-pathway inhibition of YAP-TEAD activity, which controls signaling through
1258 and downstream of EGFR to the cyclin D1/p27 ratio.
1259 **H)** Model proposing transitions between low and high YAP-TEAD activity as contact inhibition is
1260 temporarily reduced then recovered after a delay during epithelial sheet regeneration.
1261 For all representative binned plots, data are pooled from at least 2 wells, n > 100 cells/bin,
1262 >10,000 cells/plot. All quantifications are for G1-gated cells. See also **Figure S6**.
1263

Figure S1

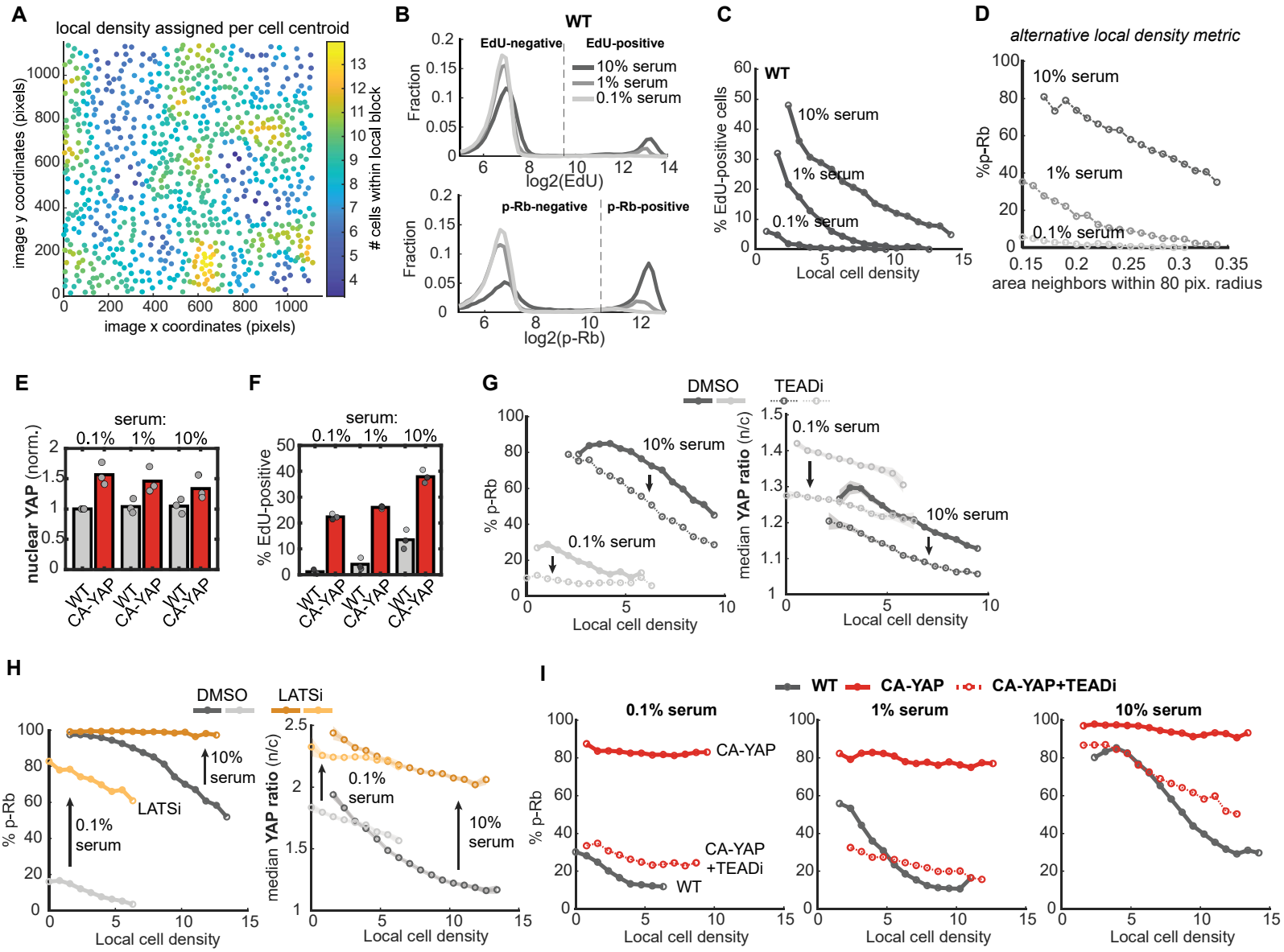
A
local density assigned per cell centroid
image y coordinates (pixels)
image x coordinates (pixels)
cells within local block
B
WT
EdU-negative
EdU-positive
10% serum
1% serum
0.1% serum
Fraction
log2(EdU)
p-Rb-negative
p-Rb-positive
log2(p-Rb)
C
WT
% EdU-positive cells
10% serum
1% serum
0.1% serum
Local cell density
D
alternative local density metric
%p-Rb
10% serum
1% serum
0.1% serum
area neighbors within 80 pix. radius
E
serum:
0.1%
1%
10%
nuclear YAP (norm.)
WT
CA-YAP
F
serum:
0.1%
1%
10%
% EdU-positive
G
DMSO
TEADi
% p-Rb
10% serum
0.1% serum
median YAP ratio (n/c)
Local cell density
H
DMSO
LATSi
% p-Rb
10% serum
LATSi
0.1% serum
median YAP ratio (n/c)
0.1% serum
10% serum
Local cell density
I
WT
CA-YAP
CA-YAP+TEADi
0.1% serum
1% serum
10% serum
% p-Rb
CA-YAP
CA-YAP +TEADi
WT
Local cell density

1264 **Figure S1, related to Figure 1**
1265
1266 **A)** Representative local density estimation in an imaging site, where circles represent the
1267 location of the centroids of cell nuclei. Cell location coordinates were divided into a 10 x 10,
1268 equally-spaced grid (local density blocks). The z-scale color indicates the number of cell
1269 centroids within a block. Cells were assigned local densities based on the number of cells in
1270 their block, scaled by the image size to give a relative density unit. See also *STAR METHODS*.
1271 **B)** Histogram plots of binary distribution of EdU (top) and Rb phosphorylation (phospho-Rb
1272 807/811, bottom) in WT RPE1 cells with 10%, 1%, or 0.1% serum. Dashed line indicates cutoff
1273 values used to designed whether cells are EdU-positive or have phosphorylated Rb. Data are
1274 representative of 3 independent experiments (same experiment as in Figure 1C).
1275 **C)** Percent EdU-positive cells per local density bin for WT cells in titrated serum levels. Data are
1276 representative of 3 independent experiments.
1277 **D)** Percent p-Rb binned by alternate local density metric (area of neighboring cell nuclear pixels
1278 within an 80-pixel (~51.6 μm) radius) for WT cells in titrated serum, showing similar density
1279 dependence as the primary local density metric.
1280 **E)** Mean nuclear YAP protein levels in serum-titrated WT and CA-YAP cells, normalized (norm.)
1281 to WT/0.1% serum condition for each experiment, n = 3 independent experiments.
1282 **F)** Mean percent EdU-positive in WT and CA-YAP across serum conditions, n = 3 independent
1283 experiments. Student's t-test: $p = 1.01 \times 10^{-5}$ (0.1% serum), $p = 8.13 \times 10^{-5}$ (1% serum), p =
1284 7.13×10^{-4} (10% serum).
1285 **G-H)** Percent p-Rb (left) and median YAP ratio (nuclear/cytoplasmic, n/c, right) binned by local
1286 density for WT and CA-YAP cells in 0.1% and 10% serum. Cells were treated with DMSO and
1287 TEADi (1 μM GNE-7883, G, dashed lines) or LATSi (0.5 μM TDI-011536, H, orange lines) for
1288 24h. Shaded error are 95% confidence intervals, n > 15,000 cells/condition. Arrows highlight
1289 drug-mediated changes for matched serum conditions.
1290 **I)** Percent p-Rb per local density bin for WT (grey) and CA-YAP cells treated with DMSO (red)
1291 or TEADi (0.5 μM, red, dashed line) in titrated serum.
1292 All binned and histogram data are from one representative replicate of 3 independent
1293 experiments, with >100 cells/bin for binned data (n >15,000 cells/condition).
1294

Figure S2

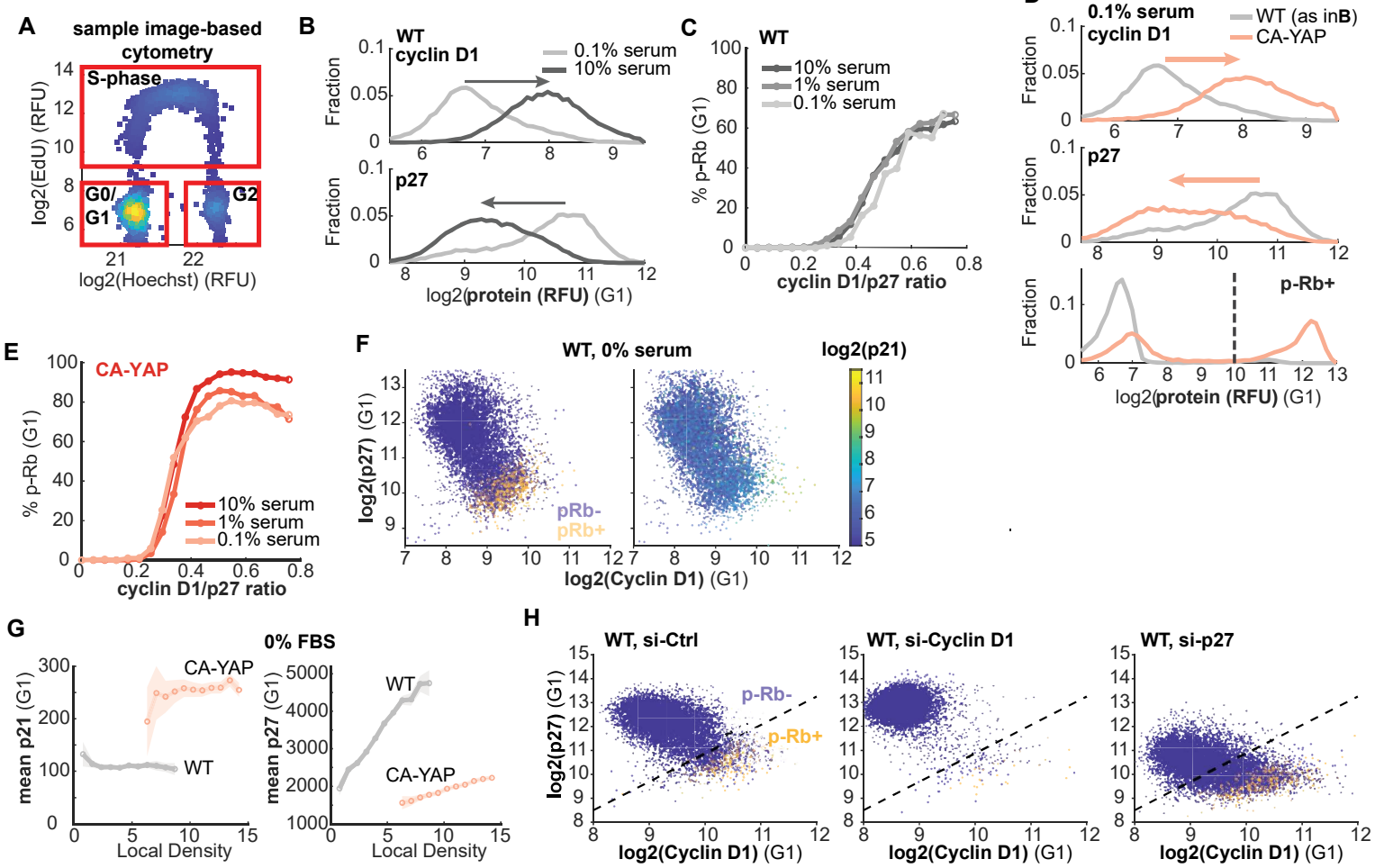
A
sample image-based cytometry
S-phase
G0/G1
G2
log2(EdU) (RFU)
log2(Hoechst) (RFU)
B
WT
cyclin D1
0.1% serum
10% serum
p27
Fraction
log2(protein (RFU) (G1)
C
WT
10% serum
1% serum
0.1% serum
% p-Rb (G1)
cyclin D1/p27 ratio
D
0.1% serum
cyclin D1
WT (as in B)
CA-YAP
p27
p-Rb+
Fraction
log2(protein (RFU) (G1)
E
CA-YAP
10% serum
1% serum
0.1% serum
% p-Rb (G1)
cyclin D1/p27 ratio
F
WT, 0% serum
log2(p21)
pRb-
pRb+
log2(p27) (G1)
log2(Cyclin D1) (G1)
G
0% FBS
CA-YAP
WT
mean p21 (G1)
mean p27 (G1)
Local Density
H
WT, si-Ctrl
WT, si-Cyclin D1
WT, si-p27
p-Rb-
p-Rb+
log2(p27) (G1)
log2(Cyclin D1) (G1)

1295 **Figure S2, related to Figure 2**
1296
1297 **A)** Density scatterplot of DNA content (Hoechst staining, real fluorescence units (RFU)) and
1298 EdU-incorporation for representative G0/G1 gating of cells. G1 population cells were defined as
1299 2N DNA/EdU-negative, S-cells as EdU-positive, and G2 as 4N DNA/EdU-negative. All-cell
1300 gating reflects cells within the outer red boundary (n = 8,000 random cells).
1301 **B)** Histogram distribution of cyclin D1 protein (top) and p27 protein (bottom) stain in WT cells in
1302 0.1% or 10% FBS. Data are representative of n = 2 independent experiments
1303 **C)** Percent p-Rb binned by cyclin D1/p27 ratio for serum titration in WT cells (n > 15,000
1304 cells/condition).
1305 **D)** Histogram distribution of cyclin D1 (top), p27 (middle), and p-Rb (bottom) stain comparing
1306 CA-YAP cells with WT in 0.1% FBS (same WT data as S1B), n > 20,000 cells/condition. Dashed
1307 line indicates p-Rb cutoff.
1308 **E)** Percent p-Rb binned by cyclin D1/p27 ratio for serum titration in CA-YAP cells (n > 15,000
1309 cells/condition).
1310 **F)** Density scatterplot of cyclin D1 stain against p27 stain, colored by binary p-Rb status (left) or
1311 p21 stain (right, parula scale) in starved WT cell.
1312 **G)** Mean p21 (left) and p27 (right) protein levels (RFU) binned by local density for starved WT
1313 (grey), and CA-YAP (red) cells (n > 20,000 cells/condition). Shaded error are 95% confidence
1314 intervals.
1315 **H)** Density scatterplots of cyclin D1 and p27 protein levels (RFU) colored by p-Rb status for
1316 serum-starved WT cells transfected with siRNA against control (si-Ctrl, left), cyclin D1 (si-Cyclin
1317 D1, middle), or p27 (si-p27, right). Dashed, diagonal line visually approximates where p-Rb
1318 bifurcates in CA-YAP conditions (matching Figure 2H).
1319 All data representative of 2 independent experiments and gated for G1-phase. All single-cell
1320 scatterplots show n = 8,000 cells.
1321

Figure S3

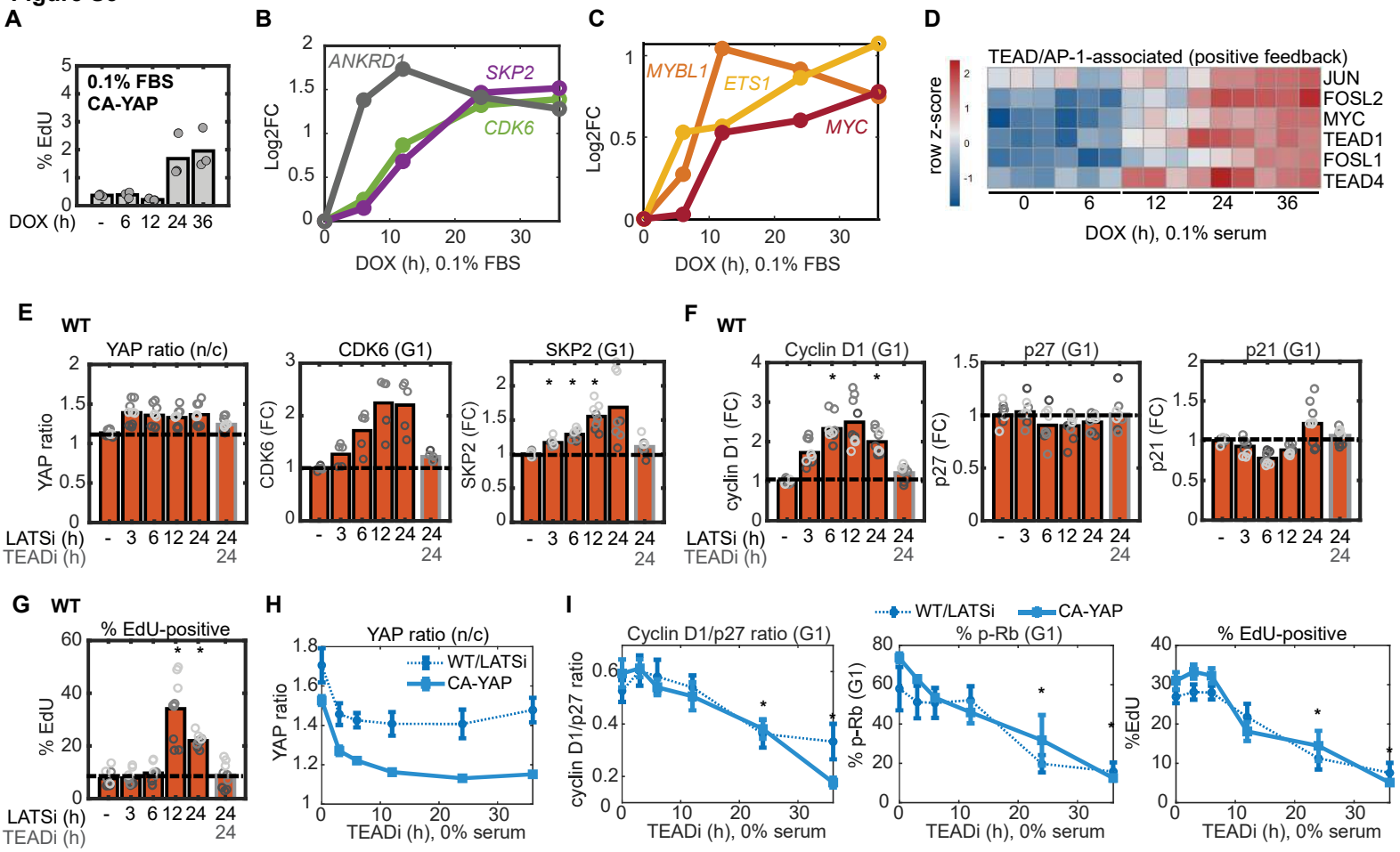
A
0.1% FBS
CA-YAP
% EdU
DOX (h)
- 6 12 24 36
B
ANKRD1
SKP2
CDK6
Log2FC
DOX (h), 0.1% FBS
C
MYBL1
ETS1
MYC
Log2FC
DOX (h), 0.1% FBS
D
TEAD/AP-1-associated (positive feedback)
row z-score
JUN
FOSL2
MYC
TEAD1
FOSL1
TEAD4
0 6 12 24 36
DOX (h), 0.1% serum
E
WT
YAP ratio (n/c)
CDK6 (G1)
SKP2 (G1)
YAP ratio
CDK6 (FC)
SKP2 (FC)
LATSi (h)
TEADi (h)
- 3 6 12 24 24
24
F
WT
Cyclin D1 (G1)
p27 (G1)
p21 (G1)
cyclin D1 (FC)
p27 (FC)
p21 (FC)
LATSi (h)
TEADi (h)
- 3 6 12 24 24
24
G
WT
% EdU-positive
% EdU
LATSi (h)
TEADi (h)
- 3 6 12 24 24
24
H
YAP ratio (n/c)
WT/LATSi
CA-YAP
YAP ratio
TEADi (h), 0% serum
I
WT/LATSi
CA-YAP
Cyclin D1/p27 ratio (G1)
% p-Rb (G1)
% EdU-positive
cyclin D1/p27 ratio
% p-Rb (G1)
%EdU
TEADi (h), 0% serum

1322 **Figure S3, related to Figure 3**
1323
1324 **A)** Mean percent EdU for matched replicates of Figure 3A reserved for immunofluorescence
1325 staining for CA-YAP cells in 0.1% FBS and arrested with palbociclib (1μM) during treatment with
1326 DMSO (-) or doxycycline (DOX) for 0-36h. N = 3 independent experiments.
1327 **B-C)** Log2 fold-change (Log2FC) induction of ANKRD1 (canonical YAP target gene, grey)
1328 compared with *CDK6* (green) and *SKP2* (purple) (B) and transcription factor targets *MYC* (red)
1329 compared with *MYBL1* (orange) and *ETS1* (yellow) at times since overexpression (C).
1330 Adjusted p-values: *CDK6*, 0.0451 (6h), 4.22 $x10^{-22}$ (12h), 3.08 $x10^{-52}$ (24h), 3.26 $x10^{-58}$ (36h);
1331 *SKP2*, 3.78 $x10^{-13}$ (12h), 3.49 $x10^{-65}$ (24h), 1.86 $x10^{-70}$ (36h); *MYC*, 2.18$x10^{-6}$(12h), 2.39$x10^{-}$
1332 ^{8}(24h), 1.50$x10^{-13}$ (36h); *MYBL1*, 7.77$x10^{-13}$ (12h), 2.76$x10^{-10}$ (24h), 3.48$x10^{-7}$ (36h); *ETS1*,
1333 1.85$x10^{-13}$ (6h), 4.55 $x10^{-16}$(12h), 6.24$x10^{-37}$(24h), 1.23$x10^{-57}$(36h).
1334 **D)** Heatmap of TEAD/AP-1-associated positive feedback genes in DOX-treated, CA-YAP cells.
1335 Color scale indicates row z-score.
1336 **E-G)** Mean YAP ratio (E, left) and fold-change in protein levels of CDK6 (E, middle), SKP2 (E,
1337 right), cyclin D1 (F, left), p27 (F, middle), p21 (F, right), and percent EdU (G) for serum starved,
1338 WT cells treated with LATSi (0.5 μM TDI-011536) for 0-24h or co-inhibited with TEADi (grey
1339 outline, 1 μM GNE-7883). N = 2 (CDK6) or 3 independent experiments (all other proteins).
1340 Student's one-sample t-test: SKP2, p = 0.0159 (3h), 0.0178 (6h), 0.0468 (12h); cyclin D1, p =
1341 0.0168 (6h), 0.0271 (24h); EdU, p = 0.0285 (12h), 6.65$x10^{-4}$ (24h).
1342 **H-I)** Mean YAP ratio (H), cyclin D1/p27 ratio (I, left), percent p-Rb (I, middle) and EdU-positive
1343 (I, right) cells following TEADi treatment of starved WT cells treated with LATSi (dashed line) or
1344 CA-YAP (solid line, same data as Figure 3I). Mean ± SEM (n = 3 independent experiments).
1345 Student's two-sample t-test, CA-YAP: cyclin D1/p27 ratio, p = 0.0354 (24h, 36h); %p-Rb, p =
1346 0.0377 (24h), 0.0328 (36h); EdU, 0.0038 (24h), 0.0012 (36h).
1347 All data are G1-gated. Colored rings indicate replicate wells within matched experimental
1348 replicates.
1349

Figure S4

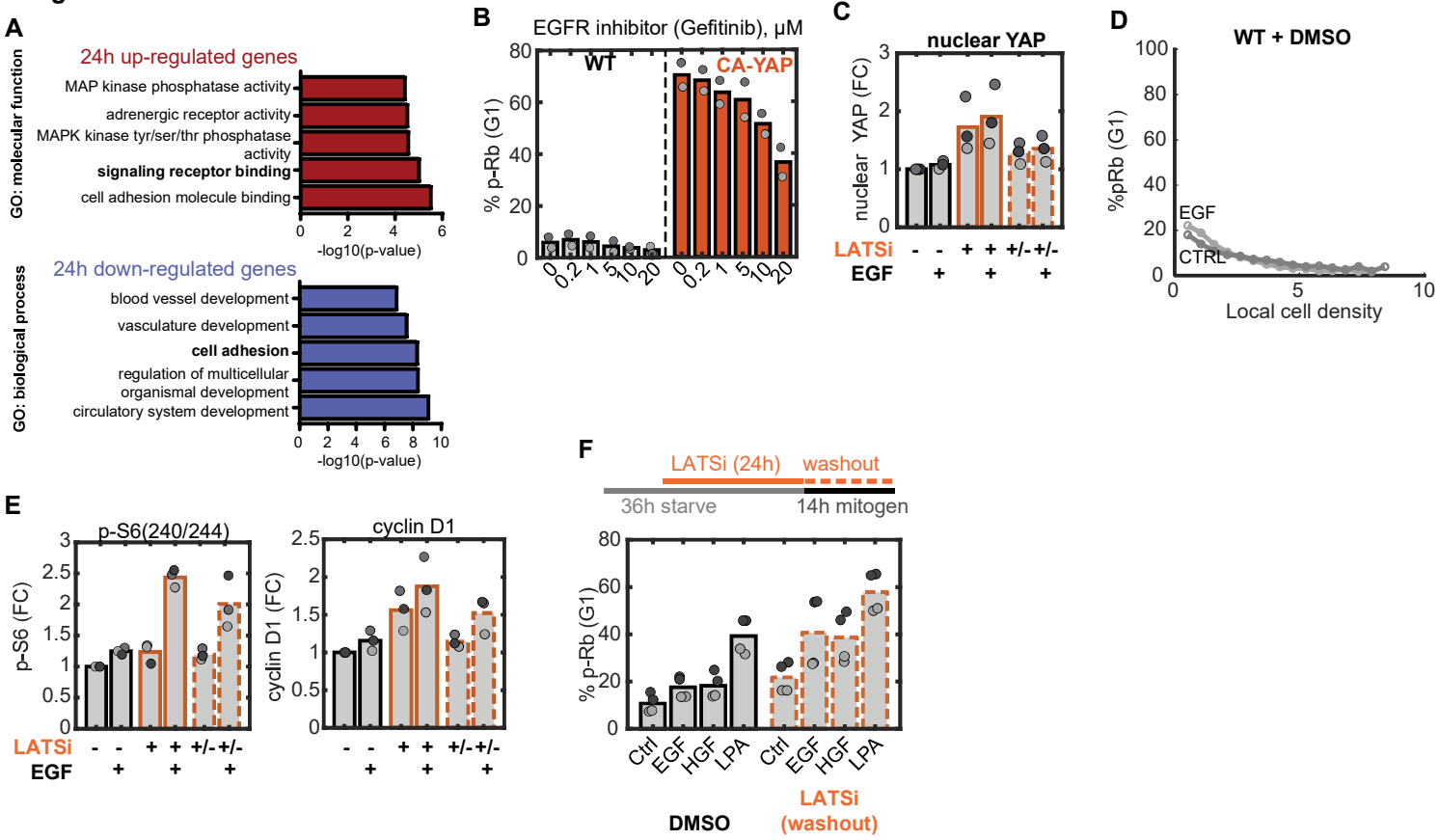
A
24h up-regulated genes
GO: molecular function
MAP kinase phosphatase activity
adrenergic receptor activity
MAPK kinase tyr/ser/thr phosphatase activity
signaling receptor binding
cell adhesion molecule binding
-log10(p-value)
24h down-regulated genes
GO: biological process
blood vessel development
vasculature development
cell adhesion
regulation of multicellular organismal development
circulatory system development
-log10(p-value)
B
EGFR inhibitor (Gefitinib), μM
WT
CA-YAP
% p-Rb (G1)
C
nuclear YAP
nuclear YAP (FC)
LATSi
EGF
D
WT + DMSO
%pRb (G1)
EGF
CTRL
Local cell density
E
p-S6(240/244)
p-S6 (FC)
cyclin D1
cyclin D1 (FC)
LATSi
EGF
F
LATSi (24h)
washout
36h starve
14h mitogen
% p-Rb (G1)
Ctrl
EGF
HGF
LPA
DMSO
LATSi (washout)

1350 **Figure S4, related to Figure 4**
1351
1352 **A)** Top: GO terms enriched for significantly up-regulated genes after 24-hour YAP induction ($q <$
1353 0.05, Log2FC > 1.0) relative to control (0.1 % FBS) (Figure 5A). Bottom: GO process terms
1354 enriched for significantly down-regulated genes ($q < 0.05$, Log2FC < -1.0).
1355 **B)** Mean percent p-Rb for serum-starved WT and CA-YAP cells treated with gefinitib (EGFR
1356 inhibitor) at indicated doses (μM) for 24h (n = 2 independent experiments).
1357 **C)** Mean fold-change in nuclear YAP levels for WT cells treated with DMSO or LATSi ± washout
1358 during EGF treatment (0.5 μM TDI-011536, 25 ng/mL EGF) as in Figure 4G (n = 3 independent
1359 experiments).
1360 **D)** Percent p-Rb binned by local density for serum-starved WT cells pre-treated with DMSO
1361 prior to 14h EGF (25 ng/mL) or control (CTRL) treatment, as in Figure 4G. Data are
1362 representative of 3 independent experiments (n > 25,000 cells/condition).
1363 **E)** Mean fold-change in cytoplasmic p-S6 (240/244, left) and cyclin D1 (right) for cells treated as
1364 in (E), G1-gated (n = 3 independent experiments, where matched colors indicate values from
1365 same experiment).
1366 **F)** Mean percent p-Rb for serum-starved WT cells pre-treated with DMSO or LATSi (5 μM,
1367 TRULI) for 24h prior to washout and 14h mitogen treatment (25 ng/mL EGF and HGF, 1 μM
1368 LPA). N = 2 independent experiments, where matched colors indicate well-
1369 replicates/experiment.
1370 All single-cell data are G1-gated cells.
1371
1372

Figure S5

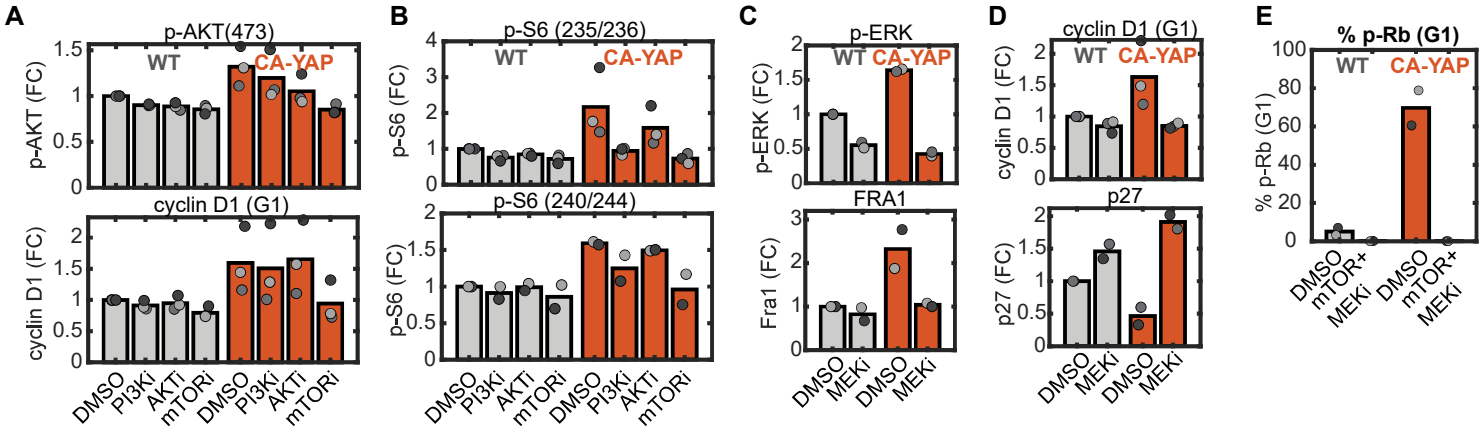
A
p-AKT(473)
WT
CA-YAP
p-AKT (FC)
cyclin D1 (G1)
cyclin D1 (FC)
DMSO
PI3Ki
AKTi
mTORi
B
p-S6 (235/236)
p-S6 (FC)
p-S6 (240/244)
C
p-ERK
p-ERK (FC)
FRA1
Fra1 (FC)
MEKi
D
p27
p27 (FC)
E
% p-Rb (G1)
% p-Rb (G1)
mTOR+
MEKi

1373 **Figure S5, related to Figure 5**
1374
1375 **A-B**) Fold-change in protein levels of p-AKT(S473) and cyclin D1 (A), and p-S6(B, top: 235/236;
1376 bottom: 240/244) for serum-starved WT and CA-YAP cells treated with PI3Ki, AKTi, or mTORi,
1377 as in Figure 5E. N = 2 (p-AKT, p-S6-240/244) or 3 (cyclin D1, p-S6-235/236) independent
1378 experiments, where matched colors indicate values from the same experiment.
1379 **C-D**) Mean fold-change in protein levels of p-ERK and Fra1 (C), cyclin D1 and p27 (D) for
1380 serum-starved WT and CA-YAP cells treated with MEKi as in Figure 5F. N = 2 (p-ERK, Fra1,
1381 p27) or 3 (cyclin D1) independent experiments, matched colors indicate values from the same
1382 experiment.
1383 **E**) Mean percent p-Rb in serum-starved WT and CA-YAP cells treated with DMSO or combined
1384 mTOR+MEKi (100 nM Torin2, 100 nM PD0325901). N = 2 independent experiments, matched
1385 colors indicate values from the same experiment.
1386 All data are from cells gated for G1-phase.
1387

Figure S6

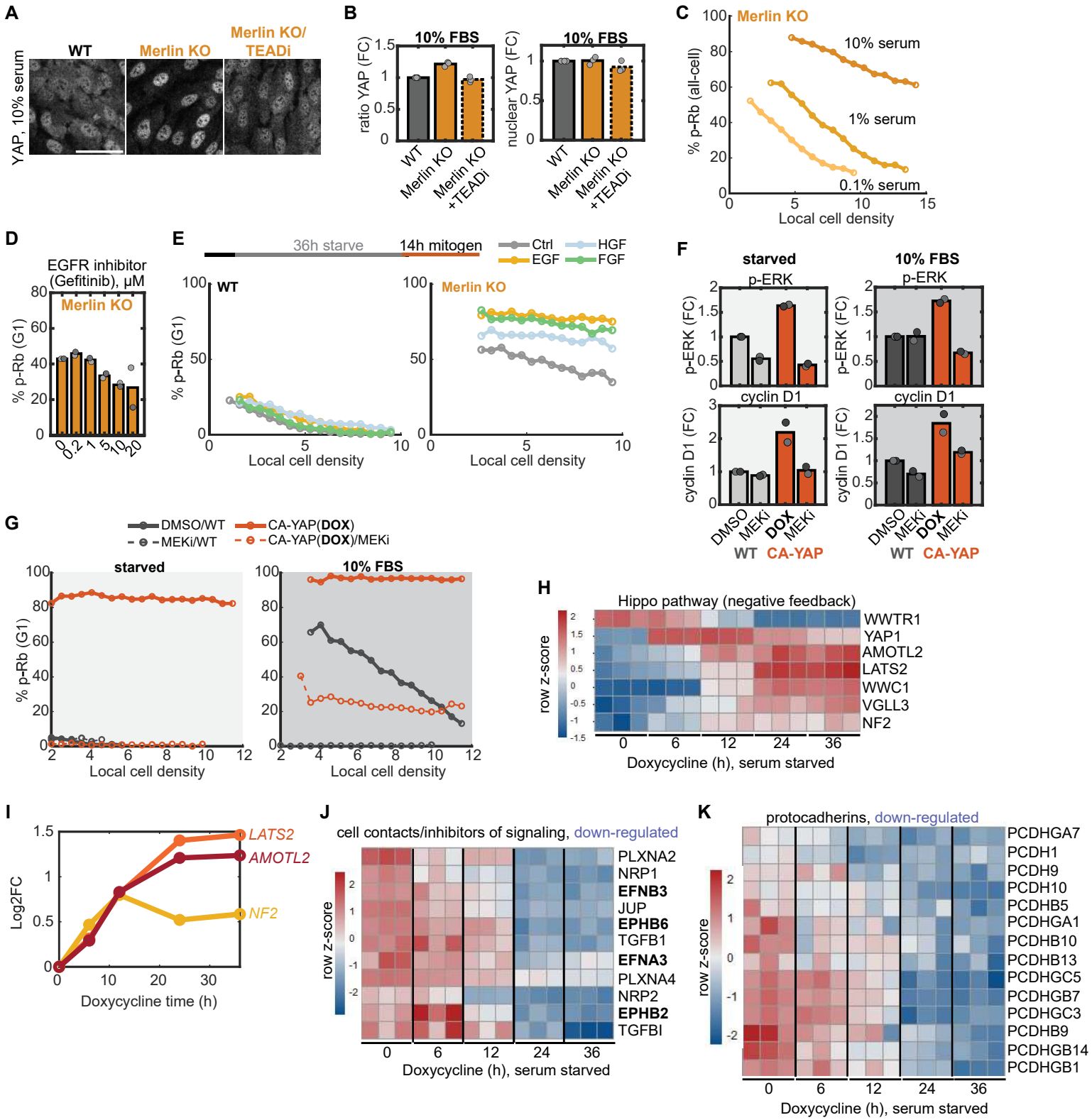
A
WT
Merlin KO
Merlin KO/ TEADi
YAP, 10% serum
B
10% FBS
ratio YAP (FC)
nuclear YAP (FC)
WT
Merlin KO
Merlin KO +TEADi
C
Merlin KO
10% serum
1% serum
0.1% serum
% p-Rb (all-cell)
Local cell density
D
EGFR inhibitor (Gefitinib), μM
Merlin KO
% p-Rb (G1)
E
36h starve
14h mitogen
Ctrl
EGF
HGF
FGF
WT
Merlin KO
% p-Rb (G1)
Local cell density
F
starved
10% FBS
p-ERK
cyclin D1
p-ERK (FC)
cyclin D1 (FC)
DMSO
MEKi
DOX
MEKi
WT
CA-YAP
G
DMSO/WT
MEKi/WT
CA-YAP(DOX)
CA-YAP(DOX)/MEKi
starved
10% FBS
% p-Rb (G1)
Local cell density
H
Hippo pathway (negative feedback)
row z-score
WWTR1
YAP1
AMOTL2
LATS2
WWC1
VGLL3
NF2
Doxycycline (h), serum starved
I
LATS2
AMOTL2
NF2
Log2FC
Doxycycline time (h)
J
cell contacts/inhibitors of signaling, down-regulated
row z-score
PLXNA2
NRP1
EFNB3
JUP
EPHB6
TGFB1
EFNA3
PLXNA4
NRP2
EPHB2
TGFBI
Doxycycline (h), serum starved
K
protocadherins, down-regulated
row z-score
PCDHGA7
PCDH1
PCDH9
PCDH10
PCDHB5
PCDHGA1
PCDHB10
PCDHB13
PCDHGC5
PCDHGB7
PCDHGC3
PCDHB9
PCDHGB14
PCDHGB1
Doxycycline (h), serum starved

1388 **Figure S6, related to Figure 6**
1389
1390 **A)** Representative immunofluorescence images of YAP staining in WT, Merlin KO, and TEADi-
1391 treated Merlin KO (0.5 μM GNE-7883) in 10% serum. Scale bar = 50 μm.
1392 **B**) Mean fold-change in YAP ratio and nuclear YAP levels in Merlin KO treated with DMSO or
1393 TEADi relative to WT cells, as in (A). N = 3 independent experiments.
1394 **C**) Percent p-Rb per local cell density bin for Merlin KO cells maintained in titrated serum levels
1395 (gating for all cells, as in Figure 1C). N > 20,000 cells/condition.
1396 **D**) Mean percent p-Rb for serum-starved Merlin KO cells treated with gefitinib (EGFR inhibitor)
1397 at indicated doses (μM) for 24h. N = 2 independent experiments.
1398 **E**) Top: starvation-release protocol for WT or Merlin KO cells with control (CTRL), EGF, HGF, or
1399 FGF (all 25 ng/mL). Bottom: percent p-Rb comparing WT (left) and Merlin KO (right) treated with
1400 CTRL or mitogens (n>12,000 cells/condition). Data are representative of 2 independent
1401 experiments.
1402 **F)** Mean fold-change in p-ERK (top) and cyclin D1 (bottom) for WT and DOX-induced CA-YAP
1403 cells treated as in Figure 5F in starvation (left) and 10% serum conditions (right). N = 2
1404 independent experiments, where matched colors indicate values from the same experiment.
1405 **G)** Percent p-Rb binned by local density for WT and DOX-induced CA-YAP cells starved (left) or
1406 in 10% serum (right) treated with DMSO or MEKi as in (F). Starved: n > 5,000 cells (WT), n >
1407 20,000 cells/condition (CA-YAP); 10% serum: n > 10,000 cells (WT), n > 20,000 cells/condition.
1408 Data are representative of 2 independent experiments.
1409 **H-I)** Heatmap of DOX-induced gene expression changes for a subset of YAP/Hippo pathway
1410 genes (H) and log2-fold change (Log2FC) in expression of *LATS2* (orange), *NF2* (Merlin,
1411 yellow), and *AMOTL2* (Angiomotin-like 2, red) over time of induction (I). Z-scale is row-count
1412 normalized z-score (H), n = 3 independent experiments.
1413 Adjusted p-values (I): *LATS2*, 0.0085 (6h), 1.09 $\times 10^{-17}$ (12h), 2.75 $\times 10^{-54}$ (24h), 1.56 $\times 10^{-59}$ (36h);
1414 *NF2*, 2.12 $\times 10^{-8}$ (6h), 1.18 $\times 10^{-25}$ (12h), 1.24 $\times 10^{-11}$ (24h), 9.16 $\times 10^{-15}$ (36h); *AMOTL2*, 0.0078
1415 (6h), 2.18 $\times 10^{-21}$ (12h), 9.00 $\times 10^{-46}$ (24h), 3.44 $\times 10^{-48}$ (36h).
1416 **J-K**) Heatmap of differential expression (row z-score) of select down-regulated inhibitory and
1417 cell-contact related genes (J) and protocadherins (K) from RNAseq, grouped by 3 independent
1418 replicates and time points.
1419 All binned data are G1-gated unless stated otherwise, with n > 100 cells/bin.